Master Thesis

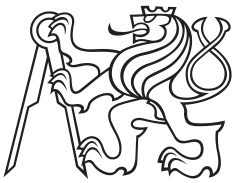

Czech Technical University in Prague

F3

Faculty of Electrical Engineering
Department of Control Engineering

Heat transfer media detection on a centrifugal pump

Bc. Ondřej Šrámek

Supervisor: Ing. Jiří Dostál
Field of study: Cybernetics and robotics
Subfield: Cybernetics and robotics
May 2020

MASTER'S THESIS ASSIGNMENT

I. Personal and study details

Student's name: **Šrámek Ondřej** Personal ID number: **457436**

Faculty / Institute: **Faculty of Electrical Engineering**

Department / Institute: **Department of Control Engineering**

Study program: **Cybernetics and Robotics**

Branch of study: **Cybernetics and Robotics**

II. Master's thesis details

Master's thesis title in English:

Heat transfer media detection on a centrifugal pump

Master's thesis title in Czech:

Detekce teplonosného média z provozních dat odstředivého čerpadla

Guidelines:

1) Study centrifugal pumps, the physics of heat transfer media, statistical detection methods.
2) Create a mathematical model of a centrifugal pump behavior for various heat transfer media.
3) Develop an algorithm for heat transfer media detection from pump operational data.
4) Verify the concept on a real pump setup.

Bibliography / sources:

[1] Gülich, J. F., Centrifugal Pumps, Berlin, Springer, 2010. ISBN 978-3-642-12824-0
[2] Papantonis, D., Centrifugal Pumps, Rijeka, InTech, 2012, ISBN 978-953-51-0051-5
[3] Havlena, V., Štecha, J., Moderní teorie řízení, Praha, Vydavatelství ČVUT, 1999.

Name and workplace of master's thesis supervisor:

Ing. Jiří Dostál, Department of Control Engineering, FEE

Name and workplace of second master's thesis supervisor or consultant:

Date of master's thesis assignment: **10.02.2020** Deadline for master's thesis submission: **22.05.2020**

Assignment valid until: **30.09.2021**

Ing. Jiří Dostál	prof. Ing. Michael Šebek, DrSc.	prof. Mgr. Petr Páta, Ph.D.
Supervisor's signature	Head of department's signature	Dean's signature

III. Assignment receipt

The student acknowledges that the master's thesis is an individual work. The student must produce his thesis without the assistance of others, with the exception of provided consultations. Within the master's thesis, the author must state the names of consultants and include a list of references.

. _____
Date of assignment receipt

_____
Student's signature

Acknowledgements

I would like to express my gratitude to the people who helped me with this work. Foremost, I would like to thank my supervisor, Ing. Jiří Dostál, whose support, inspiring suggestions and patient guidance helped towards the successful completion. I also wish to thank the CFD experts doc. Ing. Karel Petera, Ph.D. and Marek Scholler. The practical experiments would not have been possible without the help of my teammates and fellow students Ondřej, Tomáš, Jiří and Lukáš. Finally, great thanks belongs to my family who have supported me throughout my studies and during the work on this thesis.

Declaration

I declare that the presented work was developed independently and that I have listed all sources of information used within it in accordance with the methodical instructions for observing the ethical principles in the preparation of university theses.

Prague, dated on 22 May 2020

Abstract

This thesis deals with the detection of heat transfer media in one-pipe heating systems. The influence of selected properties of transported liquid on the centrifugal pump performance is analysed in the thesis introduction. Subsequently, the procedure for obtaining models of pump power dependence on the pumped fluid viscosity is presented. The pump model is then used as a basis for algorithms detecting the presence of water in the heating system, as well as estimating the viscosity of the pumped liquid. The estimated viscosity can also be used to determine the concentration of water and additive mixture to discover specific heat capacity in order to refine the heat flow estimate. The analysis of the arbitrary liquid influence on the pump performance is mediated by CFD simulations. Lastly, the functionality of proposed methods is validated using a real pump with mixtures of water and ethylene glycol in various concentrations.

Keywords: viscosity estimate, centrifugal pump, fluid detection, statistical estimation

Supervisor: Ing. Jiří Dostál

Abstrakt

Tato práce se zabývá detekcí teplonosného média jedno-trubkových otopných systémů. V úvodu práce je vyhodnocen vliv vybraných vlastností přepravované kapaliny na výkon odstředivého čerpadla. Následně je představen postup získání modelů závislosti výkonu čerpadla na viskozitě čerpané kapaliny. Tento model je poté využit jako základ pro algoritmy detekující přítomnost vody v otopném systému, a také odhadující viskozitu čerpané kapaliny. Odhad viskozity je pak možné využít pro stanovení koncentrace směsi vody a aditiva s cílem určení měrné tepelné kapacity za účelem zpřesnění odhadu tepelného toku. Pro umožnění analýzy vlivu libovolné kapaliny na výkon čerpadla jsou v této práci využity CFD simulace. Na závěr je provedena validace funkčnosti navržených metod s využitím reálného čerpadla a směsí vody a ethylen glykolu s různými koncentracemi.

Klíčová slova: odhad viskozity, odstředivé čerpadlo, detekce kapaliny, statistické odhadování

Contents

Figures

Tables

Chapter 1

Introduction

HVAC (heating, ventilation, and air conditioning) systems such as heating and cooling circuits are nowadays present in almost every building. Currently, the most popular option is a two-pipe hydronic system. The architecture of two-pipe system is shown in Figure 1.1.

Introduction of electrical circulator pumps allowed for the use of such systems not only in household and residential buildings. This system remains the most popular in Europe, but other successful variations have been introduced. Due to notable material savings, the one-pipe hydronic heating system became popular, especially in the USA and Canada.

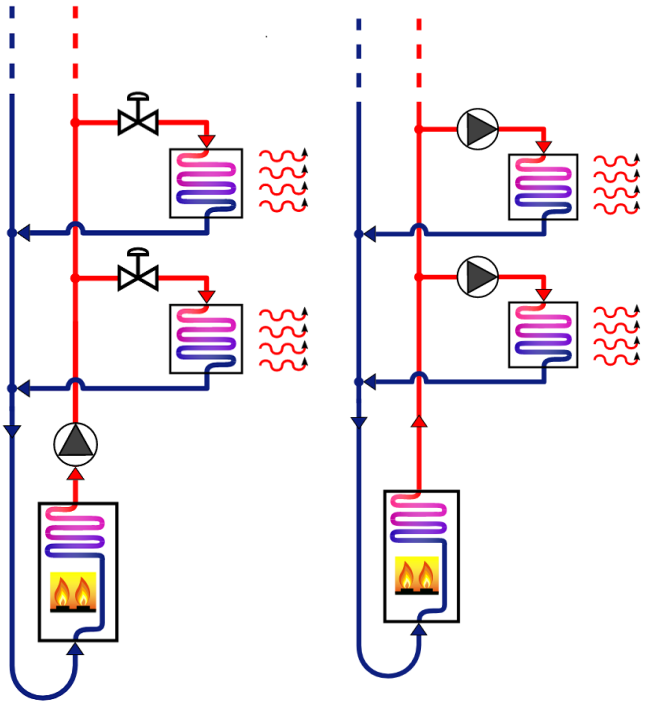

(a) : The throttling control. **(b) :** The pump control.

Figure 1.1: The two distinct heat flow control approaches for two-pipe hydronic systems.

The original one-pipe system was passive and contained just a single pump providing

the required flow. Throughout further development, the active one-pipe system was introduced. This system contains a primary pipe that ensures the transport of heat throughout the building. Secondary loops are connected to the primary pipe through a twin tee fitting. This double-tee ensures hydraulic separation of circuits. Every secondary loop has a pump, which controls flow through the heat exchangers in a given area. The principle is depicted in Figure 1.2. This system can be used for both heating and cooling based on the temperature of the flowing liquid. Properties of the active one-pipe system and their comparison to other systems are provided in an article [1].

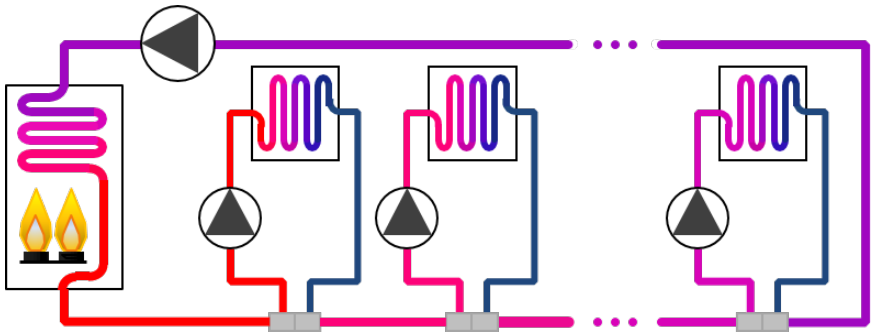

Figure 1.2: The active one-pipe hydronic system.[2]

For efficient control, it is necessary to know the viscosity and specific heat capacity of heat transfer fluid. These quantities can be determined using specialized sensors which are costly. Adding sensors to already completed systems is almost impossible due to extensive costs.

The flow through the secondary pump can be estimated using statistical estimation methods from real-time operation data of pump and temperature of flowing media fluid [3]. The estimate of actual heat flow used for control of the heating system is affected with fluid properties. Firstly, viscosity affects the accuracy of the virtual mass flow sensor. The estimate inaccuracy is caused by system hydraulic resistance change. Secondly, the heat flow also depends on the specific heat capacity. For these reasons, the determination of the fluid properties is necessary.

The goal of this thesis is to detect heat transfer media based on pump process data and develop viscosity virtual sensor.

1.1 Organization of thesis

The thesis is divided into five chapters. Firstly, the theoretical analysis of fluids, centrifugal pumps and data analysis are covered in Chapter 2. Secondly, the description of pump model properties and acquisition is discussed in Chapter 3. The heat fluid parameters estimation is described in Chapter 4. Lastly, the discussion and result analysis are done at the end of Chapter 5.

1.2 Related publications

The first related publication is the patent [4], in which the methods and system for determining viscosity of fluid are described. The estimation is done by measuring axial oscillation damping of magnetically suspended rotor of centrifugal pump. For rotor suspension The magnetic bearing is needed. This principle is developed especially for blood viscosity estimation in medical usage.

The second method of fluid viscosity estimation is published by Lloyd C. Hubbard and Earl W. Clausen in the patent [5]. This method was also developed for blood analysis in medical field. The estimation procedure, in contrary to the first patent, is divided into two steps. Firstly, the pump is operated at selected angular speed with sensing the pump torque in order to estimate blood flow. Secondly, the pump outlet is manually clamped to reduce the blood flow to zero. Due to the blood flow reduction, the viscosity factor is based upon the pump torque.

The third mentioned publication is the dissertation written by S. B. Alabi[6]. It focuses on a development and implementation of an Online Kraft Black Liquor Viscosity Soft Sensor. The artificial neural network based models developed in this dissertation were found to be superior to the traditional models in terms of accuracy, generalization capability and their applicability to a wide range of process conditions. If the parameters of the resulting artificial neural network models can be successfully correlated with the liquor composition, the models would be suitable for online application.

Chapter 2

Theoretical analysis

In view of heat flow optimal control, the heat transfer media specific heat capacity determination is of vital importance. Due to the impossibility of direct online in-process measurement, the detection and estimation algorithms developed in this thesis are based on evaluation of a fluid viscosity effect on a pump performance.

2.1 Fluid viscosity

Viscosity is a basic property of all liquids which measures the resistance to flow or shear. It can be also termed as a drag force and frictional fluid properties. Although the viscosity of liquids and gases is a function of both temperature and pressure, the manner in which it affects liquids and gasses is different.[7] For this reason, only the temperature dependence is taken into account in this thesis. Viscosity is expressed in two forms.

*"**Dynamic viscosity** is the tangential force per unit area required to slide one layer (A) against another layer (B) as shown in Figure 2.1 when the two layers are maintained at a unit distance. In Figure 2.1, force F causes layers A and B to slide at velocities v1 and v2, respectively."*[7]

The dynamic viscosity can be written as:

$$\mu = \sigma \frac{x}{v}, \tag{2.1}$$

where σ is the shear stress, x is the length and v is the velocity.[7] **Kinematic viscosity**, which requires knowledge of fluid density ρ in relation to temperature and pressure, can be defined as:

$$\nu = \frac{\mu}{\rho}. \tag{2.2}$$

The determination of viscosity is used for process quality control, while the optimum conditions of chemical processes should be met. It is also important for determination of dimensionless parameters such as Reynolds's number. The flow characteristics which are dependent mainly on the viscosity can be divided into categories:

- **Newtonian** fluid is characterized by viscosity independent of the applied shear stress.

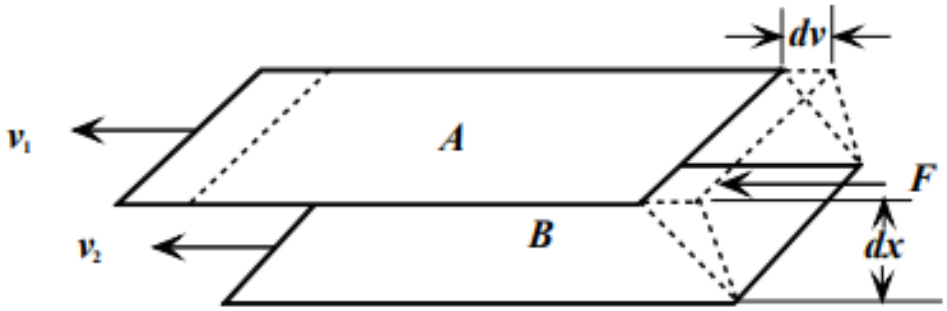

Figure 2.1: Simple shear of a liquid film.[7]

- **Non-Newtonian**, is characterized by viscosity dependent on the applied shear force and optionally on time.

2.1.1 Rheometers

Since viscosity is important in industrial processes, accurate measurements of viscosity is of vital importance. Therefore, various estimation techniques and measurement have been developed. The equipment used to measure the viscosity can be divided into seven categories of viscometers.[7]

- Capillary
- Orifice
- High temperature high shear rate
- Rotational
- Falling ball
- Vibrational
- Ultrasonic

This thesis is focused on possible fluid process detection intended for use in an industrial environment, so only the process in-line viscometer types are described.

The **rotational** viscometers are based on the principle of measuring the rotation rate of solid part in measured medium upon application of a known torque to the solid part. The basic structure is shown in Figure 2.2. Some advantages of rotational viscometers are:

"... measurements under steady state conditions, multiple measurements with the same sample at different shear rates, continuous measurement on materials whose properties may be function of temperature, and small or no variation in the rate of shear within the sample during a measurement."[7]

The **vibrational** viscometers use the principle of measurement of the damping

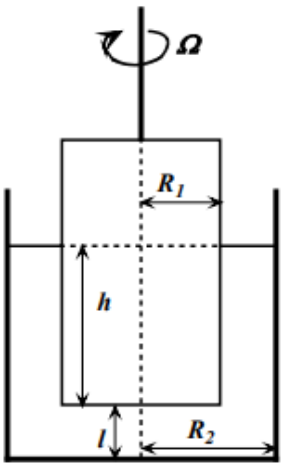

Figure 2.2: Basic structure of a coaxial cylinder viscometer [7].

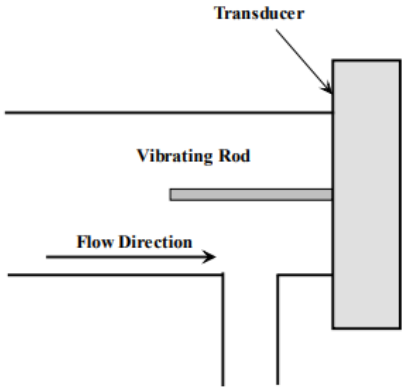

Figure 2.3: Vibrating rod system for measuring dynamic viscosity [7].

of electromechanical resonator immersed in the test liquid.

"The important features of vibrational viscometers are small sample volume requirement, high sensitivity, ease of operation, continuous readings, wide range, optional internal reference, flow through of the test liquid and consequent easy clean out and prospect of construction with easily available materials."[7]

The diagram of **vibrational** viscometer can be seen in Figure 2.3. The main disadvantage of a vibrational viscometer is its limitation to measure only dynamic viscosity. When the kinematic viscosity is required, the fluid density has to be determined independently.

The **ultrasonic** viscometers use high frequency sound waves in order to determine the instantaneous and continuous measurement of viscosity. This type of sensor can operate in a wide temperature range or in a vacuum. The schematic diagram can be seen in Figure 2.4 and also provides a further clarification. The full operating principle is described below.

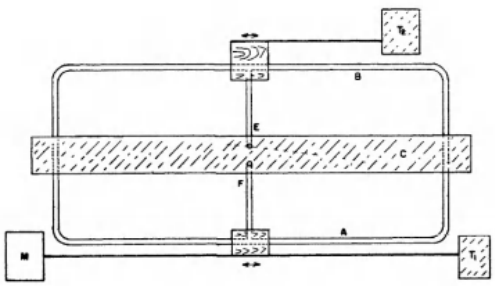

Figure 2.4: A schematic diagram of an ultrasonic viscometer [7].

"The oscillatory motion of a sphere in a viscous liquid is utilized to measure the viscosity. The device consists of two electro dynamic transformers, placed along a common axis. The coils of both the transformers are suspended in permanent electric fields and attached to each other by means of a rod. When measurements are carried out on liquids, a sphere is attached to the rod, while the viscoelastic materials are directly fixed to the end of the rod."[7]

One of the advantages of ultrasonic viscometer is its ability to reach accuracy of a few percent in the wide ranges of fluid viscosity.[7]

2.1.2 Viscosity of mixtures

The intuitive expectation of mixture viscosity as a linear function of molar, volume, or mass composition cannot be generally applicable even to the mixtures composed of substances which behaviour is nearly ideal. In real applications, certain exponential types of dependence are often observed. Since the main goal of this thesis is the heat transfer medium detection, only some empirical methods are mentioned. Firstly, computationally and informatively undemanding are for example **Kendal and Monroe relation** for mixture viscosity in form:

$$\mu_m^{\frac{1}{3}} = x_1\mu_1^{\frac{1}{3}} + x_2\mu_2^{\frac{1}{3}}, \tag{2.3}$$

or the **Arrhenius equation**:

$$log\mu_m = x_1 log\mu_1 + x_2 log\mu_2, \tag{2.4}$$

where x_1 and x_2 are mole fractions of binary mixture. These can be applicable in case of mixture components which are non-polar and non-associated, or in such cases where one of the component is present in dominant quantity. Other empirical methods include some temperature dependent interaction coefficients, volume fractions, mixture density or component molar mass. Despite the improvement of the methods, it is still an empirical approach, which in addition depends on the properties of the individual mixture components. For this reason, the estimate viscosity gives relatively huge errors which can be observed in **Tamura and Kurata equation** with an average error of 5-7 % or **Lima form of Souders' equation** with an average deviation of 12 %.[7]

For the interested in this field of study, the various methods of viscosity estimation such as usage of complex models or artificial neural networks are discussed in great detail in book Viscosity of Liquids: Theory, Estimation, Experiment, and Data.[7]

2.2 Fluid dynamics

The diverse flow phenomena occurring in blood flow in vessels, fluid flow in centrifugal pumps or global weather events can be described by only few physical laws reviewed in this chapter. The emphasis will be placed on those that are important for centrifugal pumps.

2.2.1 Conservation laws

The basis of fluid dynamics is formed by conservation laws for mass, energy, and momentum. The fact that mass, energy or momentum cannot be produced or destroyed in a closed system or control volume is described by not strictly derivable conservation laws. For all quantities mentioned above the balance equation applies as follows:

$$X_1 - X_2 + \frac{\Delta X}{\Delta t} + Z = 0, \tag{2.5}$$

where X_1 is input and X_2 acts as output. The time change of control volume is expressed as $\frac{\Delta X}{\Delta t}$. Lastly, the additional quantity (e.g. supplied or removed mass) is labeled as Z. In this form, the balance equation can be applied to both steady and unsteady processes of any complexity regardless of loss. Only the steady processes, that satisfy the $\frac{\Delta X}{\Delta t} = 0$ will be mentioned in the following subsection. The balance equation (2.5) can be further simplified to $X_1 = X_2$ as long as the system is insulated. In other words, no mass, work or heat is supplied or removed.

To fully describe the three-dimensional flow field, the conservation laws mentioned earlier are applied to an infinitesimal volume element of a flowing fluid. This allows obtaining partial differential equations (continuity and Navier-Stokes) which generally cannot be solved analytically but only numerically.

Different types of control volumes, such as streamlines, pipes or machines, are taken into account when formulating the conservation law. As long as a liquid with a velocity c_1 and density ρ_1 flows through the inlet control surface A_1, the corresponding quantities on the output control surface are described by the equation (2.6)

$$\dot{m} = \rho_1 A_1 c_1 = \rho_2 A_2 c_2 = const. \tag{2.6}$$

For incompressible flow which is secured by constant density $A_1 \times c_1 = A_2 \times c_2$ is also fulfilled. This is the continuity equation, that describes the identity of the magnitude of incoming and outgoing mass flows in case of steady conditions. The conservation of energy can be described by the first thermodynamics law. This description is conditioned by substituting the sum of input or output mechanical power P and thermal power P_W for Z.

$$\dot{m}_1 h_{Tot,1} + \dot{m}_2 h_{Tot,2} + P_W + P = 0. \tag{2.7}$$

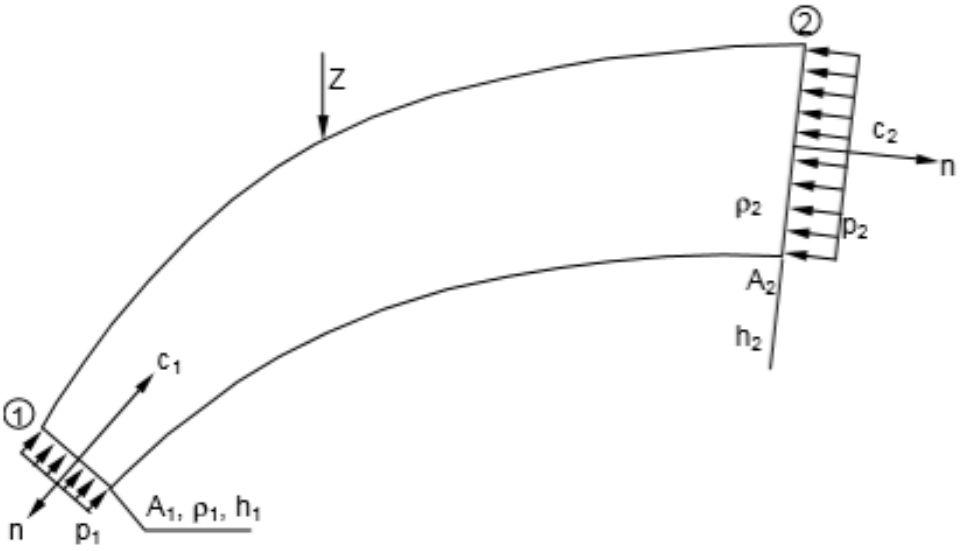

Figure 2.5: Conservation of mass, energy and momentum.[8]

The total enthalpy h_{Tot} can be expressed by the equation (2.8)

$$h_{Tot,1} = U + \frac{p}{\rho} + \frac{c^2}{2} + gz \tag{2.8}$$

where U is internal energy per unit mass, $\frac{p}{\rho}$ as the static pressure energy, $\frac{c^2}{2}$ as kinetic energy and potential energy gz. Provided that the mass flow at the inlet and outlet are equal, the turbo-machine power is obtained as the product of mass flow and the difference of the total enthalpies at inlet and outlet as follows:

$$P_i = U + \dot{m}\left(h_{Tot,2} - h_{Tot,1}\right). \tag{2.9}$$

The sum of mechanical energy transmitted to the fluid and all losses that cause heating up the fluid are considered as internal power P_i. In case of usage high-pressure pumps or turbo-machines with compressible flows, the general form has to be utilized. The enthalpy difference can be written as follows:

$$\Delta h_{Tot,1} = \frac{P_i}{\dot{m}} = U_2 - U_1 + \frac{p_2 - p_1}{\rho} + \frac{{c_2}^2 - {c_1}^2}{2} + g(z_2 - z_1). \tag{2.10}$$

The change in internal energy is caused solely by heating due to machine or volume losses. This is a result of neglecting heat exchange with environment. However, this applies only if the flow is incompressible. In this case is possible to set $U_2 - U_1 = \frac{\Delta p_v}{\rho}$. The energy on a streamline without transmission of external work ($\Delta h_{Tot} = 0$) is described by equation (2.10) which follows the first thermodynamic law.

$$p_1 + \frac{\rho}{2}{c_1}^2 + \rho g z_1 = p_2 + \frac{\rho}{2}{c_2}^2 + \rho g z_2 + \Delta p_v + \rho \int_{s_1}^{s_2} \frac{\delta c}{\delta t} ds. \tag{2.11}$$

This is Bernoulli's equation for incompressible flows. As the process is affected by losses the equation includes the loss element Δp_v. It must be used only along streamlines

or closed channels because it is assumed that the exchange of energy or mass does not occur. The equations ((2.9),(2.10)) listed above contain all the losses causing the fluid heating. When $U_2 - U_1 = \frac{\Delta p_v}{\rho}$ is replaced in equation (2.10) by hydraulic losses, the total enthalpy difference ($\Delta h_{Tot} = 0$) corresponds to the theoretical work Y_{th} of the pump as follows:

$$Y_{th} = \frac{\Delta p_v}{\rho} + \frac{p_2 - p_1}{\rho} + \frac{{c_2}^2 - {c_1}^2}{2} + g(z_2 - z_1). \tag{2.12}$$

The Y_{th} represents the work transmission to the pumped fluid per unit of mass. The losses cause generally negligible heating of the fluid whereas Y_{th} is habitually converted into useful work.

The momentum conservation for steady incompressible flows with respect to control volume as shown in the Figure 2.5 can be described as:

$$(p_1 + \rho {c_1}^2)A_1\mathbf{n_1} + (p_2 + \rho {c_2}^2)A_2\mathbf{n_2} = \mathbf{F}_{vol} + \mathbf{F}_w + \mathbf{F}_\tau. \tag{2.13}$$

where $\mathbf{n_1}$ and $\mathbf{n_2}$ are normal unit vectors directed outward to the A_1 and A_2 areas. The following equation is obtained by explicit introduction volume flow into (2.6).

$$p_1 A_1\mathbf{n_1} + \rho Q c_1\mathbf{n_1} + p_2 A_2\mathbf{n_2} + \rho Q c_2\mathbf{n_2} = \mathbf{F}_{vol} + \mathbf{F}_w + \mathbf{F}_\tau. \tag{2.14}$$

When applying the momentum conservation in the form of equations, the following conditions must be respected:

- Steady incompressible flow with uniformly distributed pressure and velocity in A_1 and A_2.
- Velocity vectors are perpendicular to A_1 and A_2.
- The unit outward directed vectors signs must be treated carefully as $\mathbf{c}_1 = -c_1 \times \mathbf{n_1}$ and $\mathbf{c}_2 = -c_2 \times \mathbf{n_2}$.
- Appropriate control volume selection, which must allow quantification of pressures and speeds on control surfaces.
- Generating indefinable forces must be avoided, if a control surface is placed through structures.

2.2.2 Curved streamlines flow

When the body or a fluid particle is supposed to move along a curved path, a force must be consequently applied to the mass, due to Newton's first law of motion. Since velocity $c(t, s)$ is a function of time and space, it can be rewritten as:

$$dc = \frac{\partial c}{\partial t}dt + \frac{\partial c}{\partial s}ds. \tag{2.15}$$

Provided that $\frac{ds}{dt} = c$, the acceleration is:

$$\frac{dc}{dt} = \frac{\partial c}{\partial t} + \frac{\partial c}{\partial s}\frac{ds}{dt} = \frac{\partial c}{\partial t} + c\frac{\partial c}{\partial s}. \tag{2.16}$$

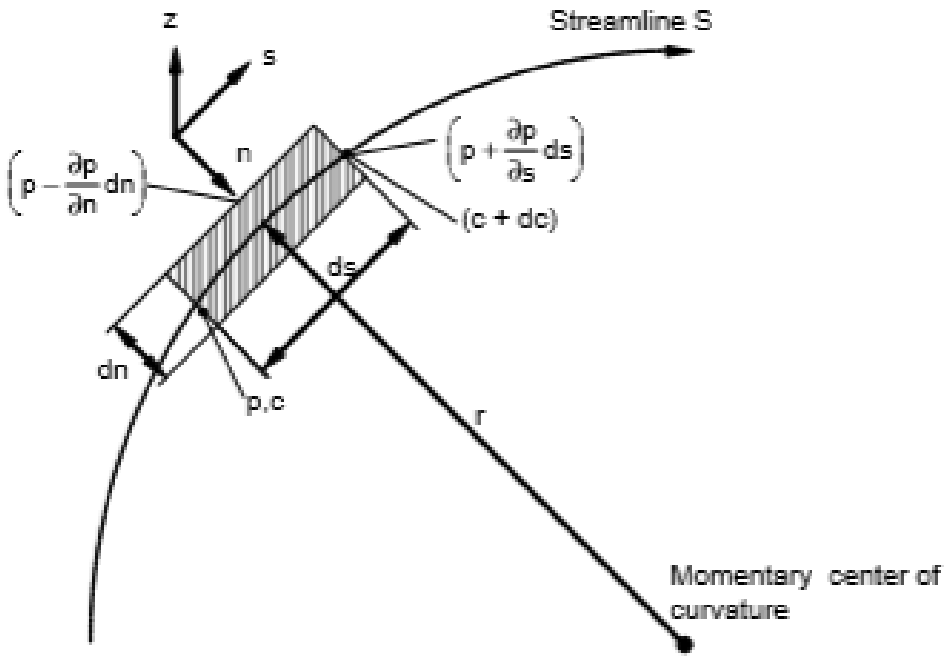

Figure 2.6: Equilibrium of forces acting on a fluid element.[8]

The acceleration normal to the streamline becomes:

$$\frac{dc_n}{dt} = \frac{\partial c_n}{\partial t} + \frac{c^2}{r} \tag{2.17}$$

if the $\frac{ds}{dt} = c$ and $\frac{\partial c_n}{\partial s} = \frac{c}{r}$. The equilibrium of perpendicular forces to the streamline is:

$$\frac{\partial c_n}{\partial t} + \frac{c^2}{r} + g\frac{\partial z}{\partial n} + \frac{1}{\rho}\frac{\partial p}{\partial n} = 0. \tag{2.18}$$

Finally, the steady flow for negligible gravity is:

$$\frac{dp}{dr} = \rho\frac{c^2}{r}. \tag{2.19}$$

According to equation (2.19) the pressure in a curved channel is decreasing from outside to inside in the direction of the center of curvature. Motion along curved path is caused by pressure gradient which imparts the necessary centripetal acceleration. The flow velocity in the center of the channel is higher than in the boundary layer. Also, the pressure gradient perpendicular to streamlines is imposed by the main flow. Accordingly, the boundary flow has to follow smaller radius than the main flow.

The fluid in the center has to be transported to outside to fulfill the condition of continuity. The flow in a section through the channel appears as a dual vortex which overlaps the main flow and results in a spiral shaped flow trajectory. The fluid particles in the center of the channel have greater velocity so they are subjected to higher centrifugal forces than slower fluid particles near the walls. Therefore, the center flow

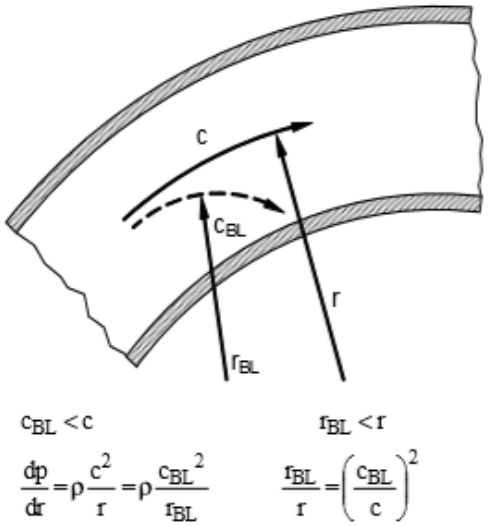

Figure 2.7: The origin of secondary flow.[8]

particles are deflected to the outside. To maintain the continuity principles, the parts will flow back to the center through boundary layer. An example of secondary flow existence can be observed along rivers, where sand is deposited inside the bend and eroded from outside. The opposite effect - sand deposits on the outer streamline due to centrifugal forces - might be expected as a result of an uninformed consideration.

2.2.3 Pressure losses

Energy losses in a flow system are caused by friction and flow separation. A fluid stall creates particularly high losses caused by the mixing of fluid with the non-separated flow.

The friction resistance is caused by non-separated boundary layers. The shear stress created by velocity gradient can be written as:

$$\tau = \rho(\nu + \nu_t)\frac{dw}{dy}, \tag{2.20}$$

where ρ is fluid density, w is relative velocity and y is dimensionless distance from the wall. Whereas the kinematic viscosity ν is a fluid property, the "eddy viscosity" ν_t depends on the structure and intensity of the turbulence. As long as $\nu_t = 0$ the flow is laminar, while $\nu_t >> \nu$ applies to turbulent flow. Due to difficulty of evaluating equation (2.20) in real practice, the wall shear stresses can be represented by friction coefficient c_f

$$\tau_0 = c_f \frac{\rho}{2} w^2. \tag{2.21}$$

The wall shear stress can also be described as a friction force dF_τ per unit area between flow and a wall element dA.

$$dP_d = w dF_\tau = \frac{1}{2}\rho c_f w^3 dA \tag{2.22}$$

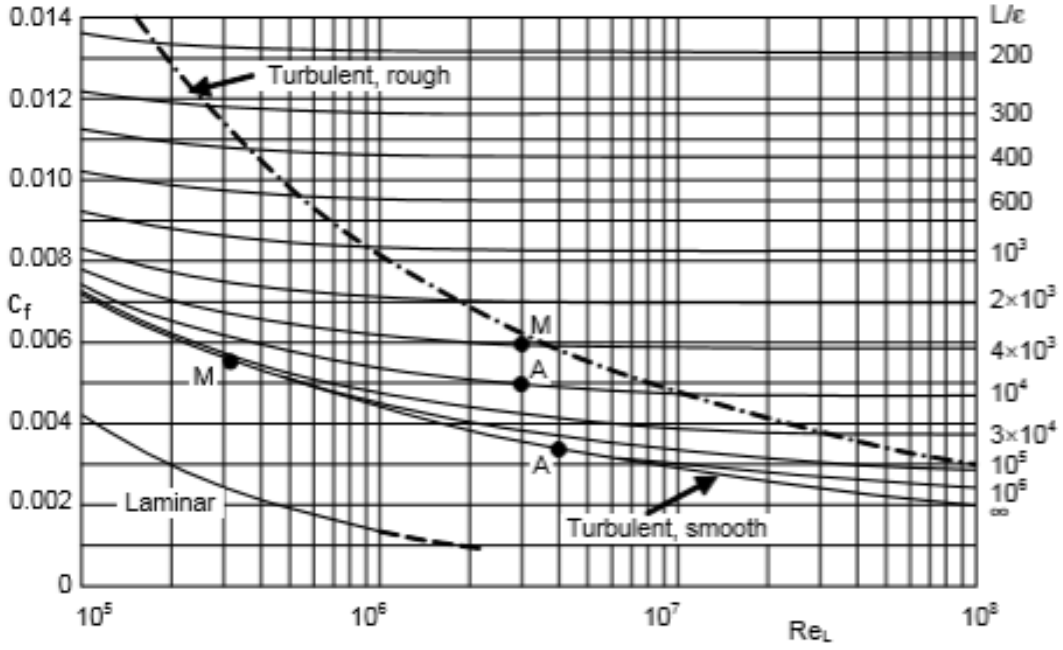

Figure 2.8: Friction coefficients c_f of flat plates in parallel flow.[8]

Hydraulically smooth	Transition roughness	Hydraulically rough
$\epsilon < \frac{100\nu}{w}$	$\frac{100\nu}{w} < \epsilon < \frac{1000\nu}{w}$	$\epsilon > \frac{1000\nu}{w}$

Table 2.1: Roughness limits ϵ.[8]

The equation (2.22) expresses the dissipated power. Since it is almost impossible to directly determine a value of the friction coefficients c_f, it must be obtained by measurements. For estimation purposes, the coefficients for flat plates are frequently used. When the flow is turbulent they can be approximately determined from equation (2.23),

$$c_f = \frac{0.136}{\left(-log\left(0.2\frac{\epsilon}{L} + \frac{12.5}{Re_L 0}\right)\right)^{2.15}} \tag{2.23}$$

with $Re_L = \frac{wL}{\nu}$. However, this equation si valid only in range of $10^5 < Re_L < 10^8$ and $0 < \frac{\epsilon}{L} < 10^{-3}$, where L is the length of the plate.[8]

Observation has revealed that roughness increases the resistance in turbulent flow. However, this is fulfilled only if the roughness elements ϵ protrude into the laminar sub-layer. If all roughness peaks do not exceed the laminar sub-layer, the wall is considered as "hydraulically smooth". On the contrary, the "hydraulically rough" walls are characterized by roughness peaks which are significantly greater than the thickens of sub-layers. The roughness limits ϵ are described in Table 2.1.

The exchange of momentum with the main flow causes the vortex shedding from the roughness peaks. The losses become independent of the Reynolds number Re and increase with the square of the flow velocity in case of fully rough domain. In the transition between smooth and rough region only the high peaks protrude

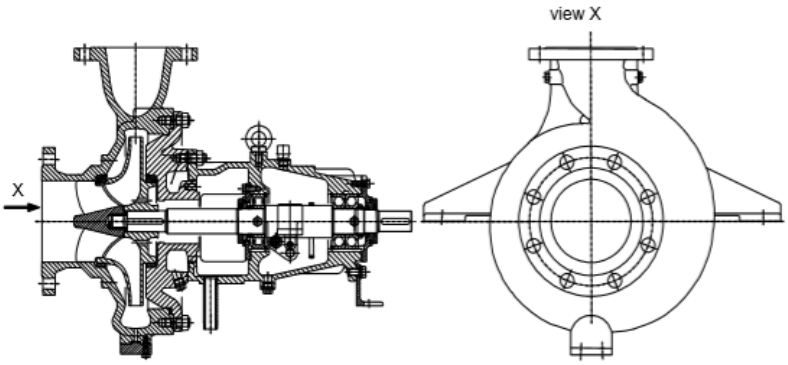

Figure 2.9: Single-stage volute pump with bearing frame [8].

through the sub-layer to turbulent domain, where there is an increase of the flow resistance which now depends on the roughness and Re. With an increasing Reynolds number the boundary layer thickness is reduced and more peaks interfere in turbulent domain.

2.3 Centrifugal pumps

Centrifugal pumps are turbo-machines used for transporting liquids. The energy transfer is usually based on hydrodynamic processes, where all pressure and energy differences are proportional to the square of the rotor speed. On the contrary, positive displacement pumps typically deliver the same volume V_{stroke} at each stroke independently of flow velocity.

The centrifugal pump is composed of a casing, a pump shaft with bearings including housing and an impeller. The pumped liquid is sucked through the suction nozzle to the impeller which is coupled with the motor. The impeller speeds up the transported liquid in the circumferential direction. Consequently, static pressure increases as the flow follows a curved trajectory. The liquid which leaves the impeller is slowed in the volute to efficiently utilize the kinetic energy at the impeller outlet to increase static pressure.

2.3.1 Pump usage

The popularity of centrifugal pumps is caused by their advantageous properties. Reliability, easy maintenance and high pressure also play a part. The possibility of pumping contaminated liquid (mud and other solid particles) cannot be neglected. Due to these properties, the centrifugal pumps are used not only across all industries, but also in households. A few typical fields of application are mentioned in the list below.

- Water distribution systems.
- Liquefaction and transport of technical gases.
- Transportation of liquids in food, petrochemical or pharmaceutical industry.

- Heating and air conditioning applications.

There are, however, some shortcomings of this pump type. On of them is its relatively small suction effect. It is also not possible to dose precise mass or volume of pumped liquid. Furthermore, this type is less efficient when it comes to viscous liquid pumping.

The pumping capabilities are affected by the construction. In order to provide the best possible performance, different component's architecture is used. The parts whose shape and properties are combined to achieve the optimal performance for different setup are listed below.

- Impeller form - radial, semi-axial and axial.
- Impeller type - closed, semi-open or open.
- Diffuser characteristic - radial or semi-axial.
- Inlet and outlet casing.

All these components are combined in many ways for the pump optimization. Due to high three-dimensionally surface complexity are impellers, casings and diffusers usually produced as castings. Small pumps are mostly fabricated from plastics.

2.3.2 Pump performance

All phenomena affecting the pump performance will be introduced in this section to analyze fluid impacts on pump power utilization. Firstly, the specific work Y is the total useful energy, which is passed by the pump to the fluid per unit of mass. At the same time, Y is equal to the total useful enthalpy rise Δh_{tot}. In the case of incompressible flow, the specific work can be expressed as:

$$Y = \Delta h_{tot} = \frac{p_{2,tot} - p_{1,tot}}{\rho} = gH. \tag{2.24}$$

The useful pump power is obtained by multiplying mass flow $m = \rho Q$ by the specific work Y:

$$P_u = \rho g H Q = Q \Delta p, \tag{2.25}$$

where H is head per stage, Q is volumetric flow and p is static pressure. The real power at the rotor shaft is greater because of looses in the pump. Therefore, the pump efficiency η is the ratio of both values.

$$\eta = \frac{P_u}{P} \tag{2.26}$$

The first source of power dissipation is caused by mechanical losses in bearings and shaft seals. Since these do not generally result in a heating of the fluid, this type of losses will be labeled as *external*. The magnitude depends on the design and component condition.[9] However, it can be determined that the magnitude of this type is approximately 1 % of the shaft power.[10]

Secondly, the different type of loss components is generated within the pump. All the types of losses listed bellow cause heating of the fluid, and they can be marked as *internal*.

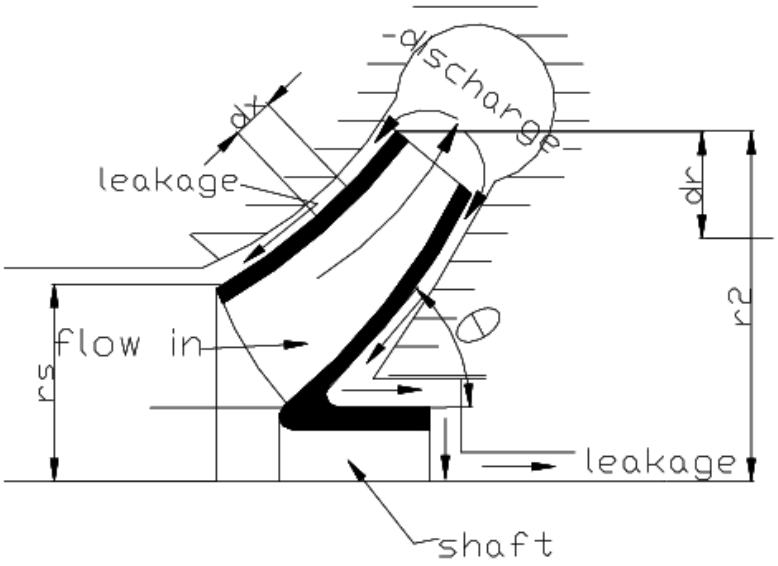

Figure 2.10: Pump sealing leakages.[10]

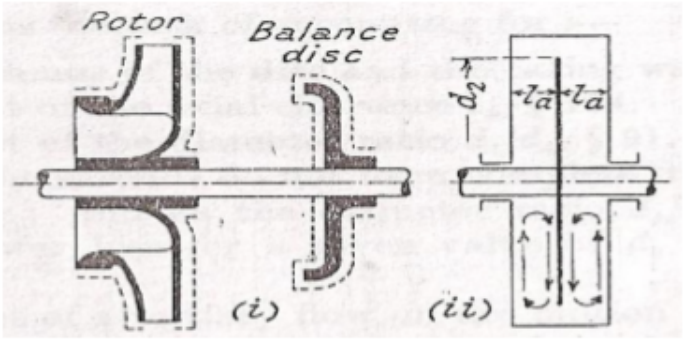

Figure 2.11: Disk friction parts.[9]

1. **Volumetric losses** caused by leakages which are pumped by the impeller. These include leakages through sealing parts. This phenomena is described in Figure 2.10 and must be supplied by power P_L which is designated in Figure 2.12.

2. **Disk friction losses** occur on the front and rear shrouds of the impeller which is rotating in the fluid. Components responsible for friction can be seen in Figure 2.11. Same phenomena arises on a balancing disk. The dissipated power is named P_{RR}.

3. **Hydraulic looses** caused by friction and turbulent dissipation in parts between suction and discharge nozzle. The diffused power is marked as P_{vh}.

4. **Fluid re-circulation** generates high losses P_{Rec} due to momentum exchange between stalled and non-separated fluid zones at part-load. With proper design this loss type should be zero, if pump operates close and above to the best

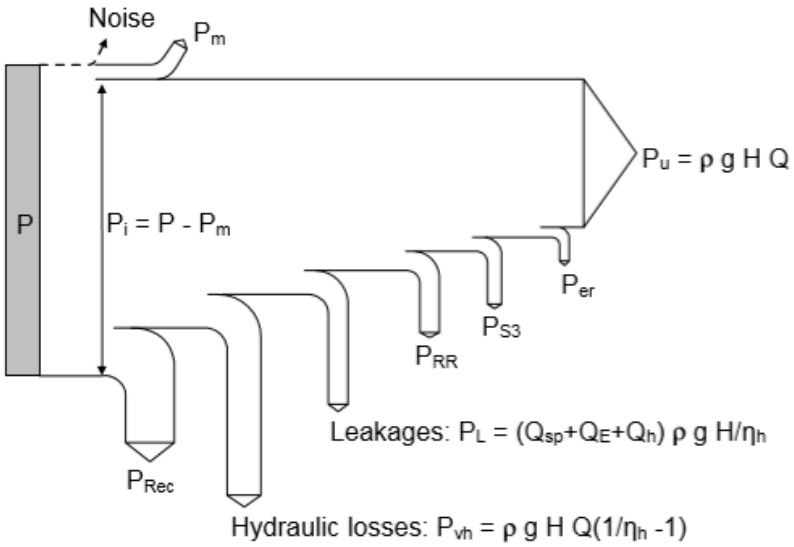

Figure 2.12: Pump power balance.[8]

efficiency point. In case of operation against closed valve or at low flow, it causes the **greatest part** of power consumption.[8]

2.3.3 Internal loss determination

In this section, losses involved in the power dissipation in closed valve working mode are discussed. This setup is optimal for fluid properties estimation because the actual flow rate measurement is not necessary.

When a disk or a cylinder rotates in fluid, the shear stress arises on its surface. In case of stationary fluid without impacts on pump housing, the shear stress can be written as:

$$\tau = \frac{\rho c_f u^2}{2}, \tag{2.27}$$

where ρ is fluid density, c_f is a Reynolds number dependent friction coefficient and u is peripheral rotating disk velocity, determined as $u = \omega \times R$. The torque exercised by friction becomes:

$$dM = r \times dF = r \times \tau dA = \pi \rho c_f r^4 \omega^2 dr. \tag{2.28}$$

The friction power per side of disk is obtained as:

$$P_{RR} = \omega \times \int_{r_1}^{r_2} dM = \frac{\pi \rho c_f \omega^3 {r_2}^5}{5} \left(1 - \frac{{r_1}^5}{{r_2}^5}\right). \tag{2.29}$$

When disk rotates inside a casing as in the case of a pump, the velocity distribution between parts is dependent on the impeller and casing distance as well as on boundary layers that appear on stationary and rotating surfaces. The disk friction represents a high proportion of total losses in centrifugal pumps, especially of the radial type. Due to this fact, the friction has a great effect on pump efficiency.[10]

The presence of re-circulation is recognized by existence of negative meridional velocities near the outer streamline. With growing back-flow from the impeller, the circumferential velocity components increase because the angular momentum is transmitted to the recirculating fluids by the blade. Furthermore, increasing losses are also caused by the rotation of recirculating fluid which is partially dissipated into a suction chamber. The recirculating fluid flow rate is obtained as:

$$Q_{Rec} = 2\pi \int c_{1m} r dr. \tag{2.30}$$

The flow angular momentum can be written in the form:

$$M_{Rec} = 2\pi\rho \int c_{1m} c_{1u} r^2 dr. \tag{2.31}$$

Lastly, the dissipated re-circulation power $P_{Rec} = \omega \times M_{Rec}$. The effect of fluid parameters on pump power consumption can be defined as:

$$P_S = \frac{\rho g Q H}{\mu_v \mu_h} + P_{df} + P_m. \tag{2.32}$$

The pump power differences caused by increasing viscosity are influenced by phenomena listed below.[11]

- With increasing friction factor the fluid leakage decreases.
- Increasing Reynolds number causes the increase of the hydraulic performance.
- Disc friction losses on impeller surface increase with growing viscosity.
- The mechanical losses are independent on transported fluid viscosity.

2.4 Data analysis

Since all measurement provided by physical sensors are burdened with noise, a statistical analysis and estimation should be utilized. All methods used in this thesis are mentioned in subsections below.

2.4.1 Probability distributions

In the theory of probability and statistics, a probability distribution is the function that provides the occurrence probabilities of different possible outcomes of an experiment.

Firstly, the standard normal distribution is shortly introduces. This distribution is in this thesis marked as $\mathcal{N}$ and it is defined by parameters μ and σ. The first moment is equal to μ, second is σ^2.

Secondly, the uniform distribution is used. It is parameterized as $\mathcal{U}(a, b)$, where a is lower limit and b is upper limit. The distribution mean can be calculated as $\frac{1}{2}(a + b)$ and variance is equal to $\frac{1}{12}(b - a)^2$.

Lastly, the t Location-Scale distribution $\mathcal{T}$ is root of Location-Scale families described on web site written by Kyle Siegrist [12]. It is parameterized by three parameters listed in Table 2.2. The normal distribution is approximated when υ goes to infinity whereas small values yield heavier tails. The mean is equal to μ and variance can be written as:

$$var = \sigma^2 \frac{\upsilon}{\upsilon - 2}. \tag{2.33}$$

Parameter	Description	Support
μ	Location parameter	$-\infty < \mu < \infty$
σ	Scale parameter	$\sigma > 0$
υ	Shape parameter	$\upsilon > 0$

Table 2.2: The t Location-Scale distribution parameters.[13]

	Status of H_0	
Decision	H_0 **- true**	H_0 **- false**
Retain	Correct decision	Type II error (miss)
Reject	Type I error (false alarm)	Correct decision

Table 2.3: Hypothesis test outcomes.[14]

2.4.2 Hypothesis testing

Statistical hypothesis test is a method used for inference evaluating. Usually by comparing two data sets, or verifying that the experimental data samples meet the specified probability distribution. The two hypotheses, the null hypothesis H_0 and the alternative one H_1 usually exist and are tested by wide range of methods. The hypotheses testing is used for experiment results evaluation or for industrial process analysis. In this thesis, the hypothesis testing has been used for fluid type detection. The three possible tests are shown in Figure 2.13. Due to the existence of various methods used for finding test parameters, mentioned in subsection 2.4.3, only the Likelihood ratio test is described in subsection 2.4.4.

2.4.3 Test quality

The quality of a hypothetical test is determined by parameters listed below.

1. Level of **significance** α indicates the probability of incorrect rejection of the true hypothesis H_0. In literature it is frequently marked as error type I. Although the level can be set arbitrarily, in most cases the 0.05 or 0.01 levels are commonly used.[14].

2. The test **Power** determines the probability $1 - \beta$ of non-rejection of a false null hypothesis H_0. As with the previous parameter, the test power can be selected arbitrarily from $(0, 1)$, however, the power is usually 0.8, in order to avoid larger sample size required for tests with higher power such as 0.9 or 0.95.[14]

3. **Sample size** determines the minimal value of independent measured samples in order to reach the test significance level and power with effect size. The effect size is defined as the difference in the parameter of interest that represents a clinically meaningful difference.

All possible decisions are listed in Table 2.3. In case of standard normal distribution and change of mean value, it is possible to estimate the sample size by formula as follows:

$$n = \left(\frac{Z_{1-\alpha/2} + Z_{1-\beta}}{ES} \right), \tag{2.34}$$

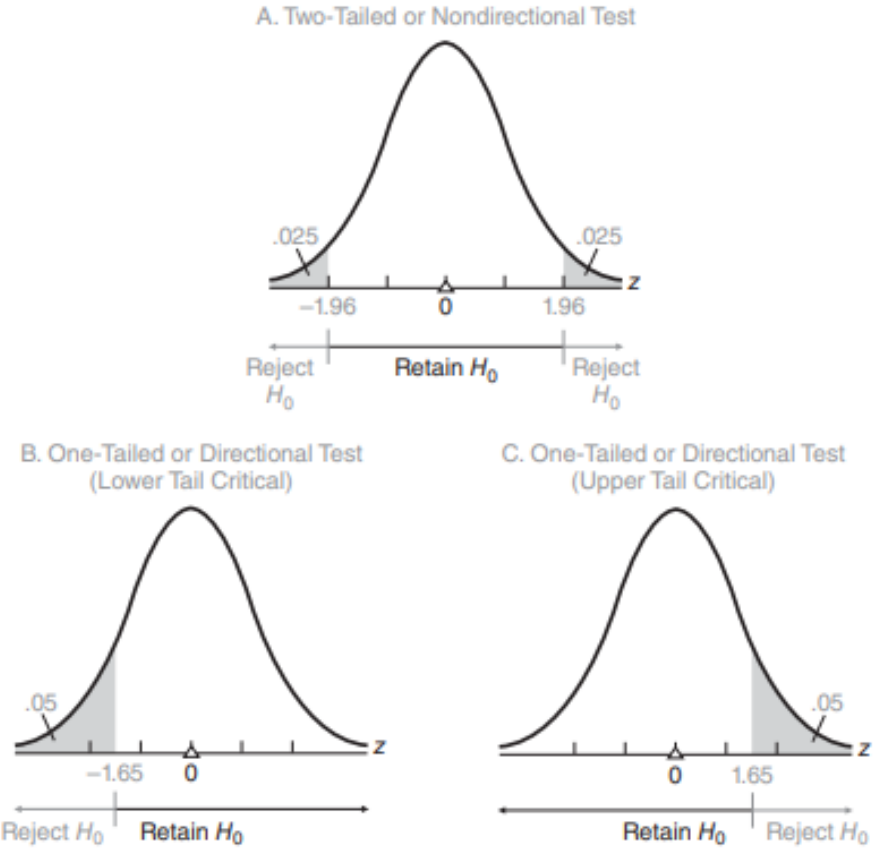

Figure 2.13: Three type of test with significance level 0.05.[14]

where $Z_{1-\alpha/2}$ is the value from the standard normal distribution holding the significance level below. In the same way the $Z_{1-\beta}$ is the value from the standard normal distribution holding the test power below. Lastly the effect size can be determined as:

$$ES = \frac{|\mu_1 - \mu_0|}{\sigma}, \tag{2.35}$$

where μ is mean of hypothesis and σ is standard deviation.[15] Since this principles can be used only in the case of normal distribution, for different probability distributions the numerical evaluation is used in this thesis.

2.4.4 Likelihood ratio

The likelihood ratio is a statistical test used for assessing the goodness of fit of two statistical models based on the ratio of their likelihoods. The first principle is demonstrated by Bayesian approach with the assumption that two hypothesis with prior probabilities $P(H_0)$ and $P(H_1)$, where $P(H_0) = P(H_1) = \frac{1}{2}$ and x is random variable. In the next step, the ratio:

$$\frac{P(H_0|\mathbf{x})}{P(H_1|\mathbf{x})} = \frac{P(H_0)P(\mathbf{x}|H_0)}{P(H_1)P(\mathbf{x}|H_1)} \tag{2.36}$$

is the product of prior probabilities and the likelihood ratio. The null hypothesis H_0 acceptance based on larger posterior probability, is either ratio value:

$$\frac{P(H_0|\mathbf{x})}{P(H_1|\mathbf{x})} = \frac{P(H_0)P(\mathbf{x}|H_0)}{P(H_1)P(\mathbf{x}|H_1)} > 1, \tag{2.37}$$

or equivalently:

$$\frac{P(\mathbf{x}|H_0)}{P(\mathbf{x}|H_1)} > c, \tag{2.38}$$

where c, the critical value, is dependent on the prior probability. The theory of hypothesis testing by decision problem making was formulated by Neyman and Pearson. The advantage of this approach is the possibility to bypass the necessity of specifying prior probability.[16] The full formulation of Neyman-Pearson lemma is:

"Suppose that H_0 and H_1 are simple hypotheses and that the test that rejects H_0 whenever the likelihood ratio is less than c and significance level α. Then any other test for which the significance level is less than or equal to α has power less than or equal to that of the likelihood ratio test."[16]

2.4.5 Maximum likelihood

Maximum Likelihood Estimation is a probabilistic framework used for solving the problem of parameter estimation. This method is appropriate in case of an unknown probability distribution of state variables. The likelihood function can be defined as:

$$l(\boldsymbol{\theta}|\boldsymbol{y}) = p(\boldsymbol{y}|\boldsymbol{\theta}). \tag{2.39}$$

The maximum likelihood estimate $\hat{\theta}_{ML}(\boldsymbol{y})$ is defined as value of $\boldsymbol{\theta}$ that maximize likelihood for observed data $\boldsymbol{y}$

$$\hat{\theta}_{ML}(y) = arg\max_{\theta} \ell(\boldsymbol{\theta}|\boldsymbol{y}). \tag{2.40}$$

Due to the usual exponential form of probability densities is in many cases advantageous to maximize the logarithm of likelihood function. If is possible to differentiate this function, the necessary condition of maximum existence in form:

$$\frac{\partial ln\, \ell(\boldsymbol{\theta}|\boldsymbol{y})}{\partial \boldsymbol{\theta}}\bigg|_{\theta=\hat{\theta}_{ML}} = 0, \tag{2.41}$$

can be named as likelihood equation. [17]

Lastly, the variance of the estimate $\hat{\theta}_{ML}(\boldsymbol{y})$ can be calculated by the inverse of hessian in form:

$$P_{\hat{\theta}} = -\left(\frac{\partial^2 ln\, \ell(\boldsymbol{\theta}|\boldsymbol{y})}{\partial^2 \boldsymbol{\theta}}\right)^{-1}. \tag{2.42}$$

Chapter 3

Mathematical model

This chapter describes the procedure of obtaining pump behaviour model for various heat transfer media. In the beginning, the procedure of numerical simulation is introduced, then the test-bench hardware and physical measurement are described, and finally the fluid detection and estimation models are created.

3.1 Heat transfer fluid properties

The usage of free of charge CoolProp[18] library is discussed at the start of this section. It is used for fluid solution parameters estimation. The data are also used for configuration of a real pump numerical simulation.

3.1.1 CoolProp incompressible fluids

This library is a free option to NIST REFPROP [19] and is based on the state equation of refrigerants such as CO_2, R134a, nitrogen, argon or ammonia. These equations have been verified by reference measurements made in this study.[18] The complete fitting report is available on the library web site [1]. The incompressible fluids utilized in the CoolProp library are divided into three groups:

- Pure fluids,
- Mass-based binary fluids,
- Volume-based binary fluids.

The most common fluids in this library are pure and mass-based binary mixtures. Although pure fluids offer many different types of incompressible liquids, almost all mixtures are aqueous solutions which allow evaluating volume concentration from 0.0 for pure water to 1.0 for pure substance. All fluids in the library have a reference state for enthalpy and entropy. Reference boundary conditions are listed in Table 3.1.

The part of incompressible fluids provide only a limited subset of input variables, which are $f(p,T)$, $f(p,h)$, $f(p,\rho)$ and $f(p,s)$. All functions internally iterate on $f(p,T)$, so this makes the combination by far the computationally fastest option.

[1] `http://www.coolprop.org/_downloads/054af054fd1e79a2529ec71153150193/all_incompressibles.pdf`

Quantity	Value
T_{Ref}	293.15 K
p_{Ref}	101325 Pa
h_{Ref}	0 Jkg^{-1}
s_{Ref}	0 $Jkg^{-1}K^{-1}$

Table 3.1: CoolProp reference point values.[18]

Quantity	Value
molar mass	62.068 $gmol^{-1}$
density	1.1132 gcm^{-3}
boiling point	470.4 K
melting point	260.2 K

Table 3.2: List of ethylene glycol selected properties at 298.15 K and 100 kPa.[20]

3.1.2 Fluid dataset generation

As one of the aims is to create a mathematical model of pump behaviour for various heat transfer media, the fluid variety is archived by analysing different concentrations of water-ethylene glycol solution. The EG (**E**thylene **G**lycol) used during the simulation and evaluation is named in the library named as AEG.

The EG is an organic compound with a summary formula $C_2H_6O_2$. Selected properties of EG at 20 °C and atmospheric pressure are is listed in Table 3.2. It is widely used as an additive in coolants for cars, air conditioning systems or plastics fabrication. Therefore, it is used where the cooling medium is exposed to temperatures below the freezing point of water. The EG disadvantage is its approximately halved specific heat capacity compared to water. Despite the fact that pure EG substance freezes at 260.2 K, water-ethylene glycol solutions freeze at even lower temperatures. For example, solution of water (40 %) and ethylene glycol (60 %) freezes at 228.15 K.[20]

3.2 CDF model

Computational **F**luid **D**ynamics (CFD) is a set of methods and mathematical models used for numerical fluid flow simulation. In real applications, it is not always possible to analytically analyse the system behaviour. This is impossible mainly due to the complexity or models' geometry. One of great advantages of CFD is the ability to look inside the simulated system in order to evaluate local properties of flow or stress. Another feature is the possibility to operate the system at configurations near potential damage or unsafe operating condition. Finally, the key feature is the ability to analyse the system without the necessity of its physical existence. This creates the possibility to reduce the financial and time demands of development. It is, however, a very complex tool that requires a deep understanding of computation problem setup and evaluation of results. For this reason, particular procedures and settings recommended by an external specialist have been used in this thesis.

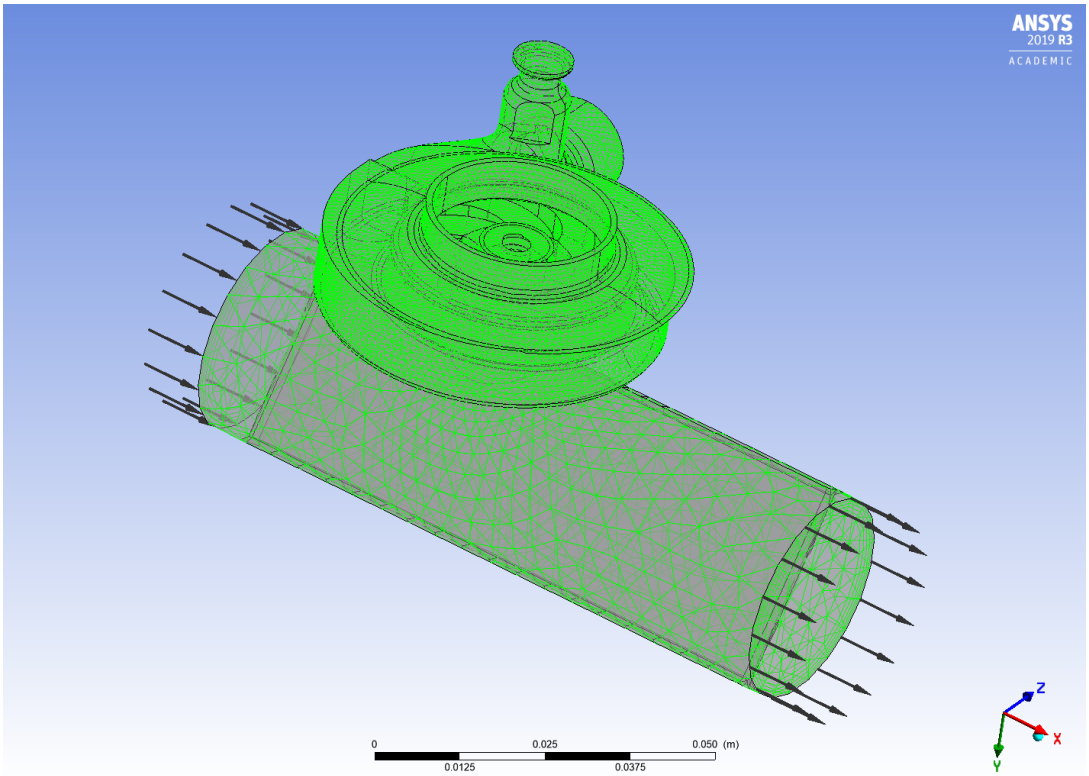

Figure 3.1: The pump model mesh in CFX Pre.

3.2.1 Simulation setup

ANSYS CFX is used for fluid analysis. It can be shortly described as:

"... the high-performance CFD software tool that delivers reliable and accurate solutions quickly and robustly across a wide range of CFD and multiphysics applications. CFX is recognized for its outstanding accuracy, robustness and speed when simulating turbomachinery, such as pumps, fans, compressors and gas and hydraulic turbines."[21]

Since the existing pump model is used for other various simulation, some geometrical parts have to be modified for this experiment. The modification is related to secondary pipeline which is replaced by stationary wall at pump outlet. The non-return spring valve used in the beginning part of the secondary pipeline in real setup is for CFD purposes replaced with this wall. The mesh of pump model is shown in Figure 3.1.

Based on observation while pretest measurement, the maximal constant pump speed is determined as speed for which non-return spring valve remains closed. This value is ideal for real fluid parameter estimation, because the impact on pump performance will be the greatest in case of zero flow.

In CFX, it is possible to evaluate a model with fully customized liquid. However, the various fluid types are created as water-ethylene glycol solution in diverse concentrations for possible comparison of experimental training data with simulation output.

The numerical simulations are designed to cover six different binary solution concentrations. The simulated fluid is also evaluated in temperature range from 25 °C to 60 °C with the step of 5 °C. The SST turbulent model is used for fluid flow

modelling. The solver is set to high resolution and first order turbulence numeric. The convergence control can run up to 10 000 iterations with time scale factor 1. Finally, the residual target is set to $1e^{-4}$.

3.2.2 Simulation results

The output of simulation results is checked in CFX by control of Courant's number and velocity streamline in the pump model. The streamlines visualization is shown in Figure 3.2. Afterwards, the output impeller torque taken as a mean of last 1000 iteration values for each calculated point. The output shaft power P is obtained by

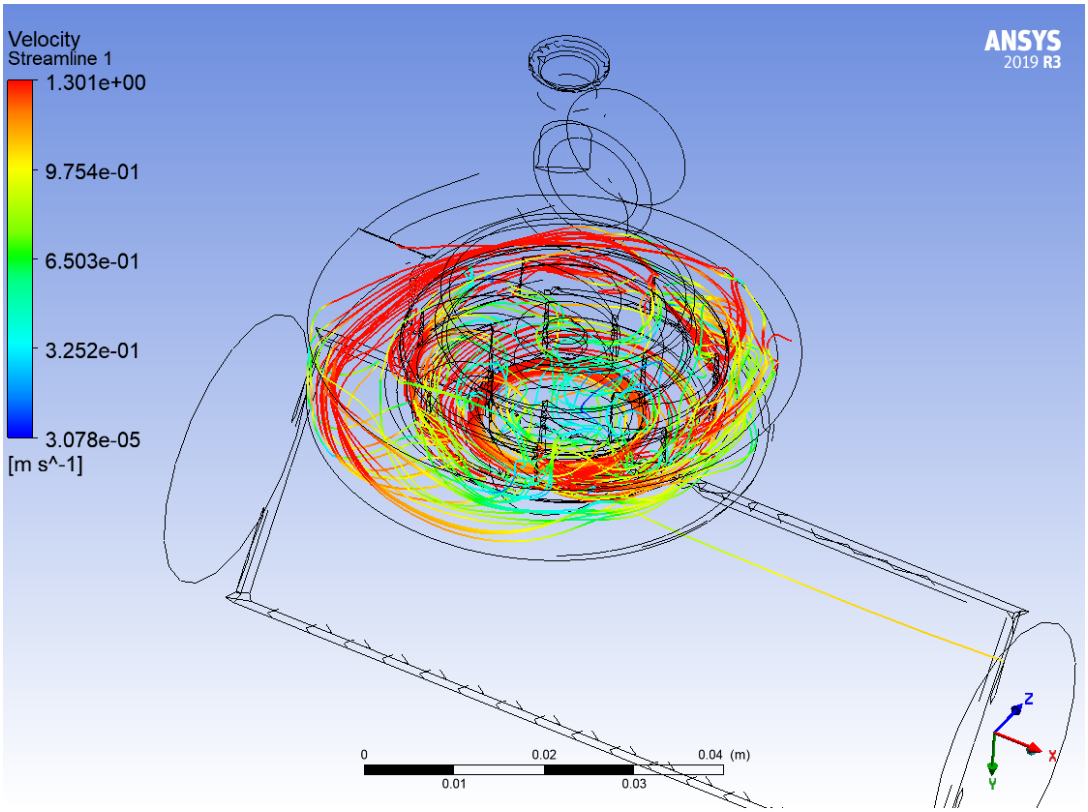

Figure 3.2: The simulation result visualization in CFX Pos.

multiplying the mean of torque τ with impeller angular speed ω in accordance with equation (3.1). These values are used to create a model of pump power dependence on fluid viscosity.

$$P = \tau\omega \tag{3.1}$$

Even though the simulation residuals depicted in Figure 3.3 and output torque in Figure 3.4 seem to be satisfactory for individual design point, overall trends do not correspond to theoretical assumptions and real measurements. Unfortunately, even after many alternations of solver settings and further consultations, simulated data still do not exhibit meaningful trends. Due to high computational complexity (approximately 10 days per run), further results could not be obtained.

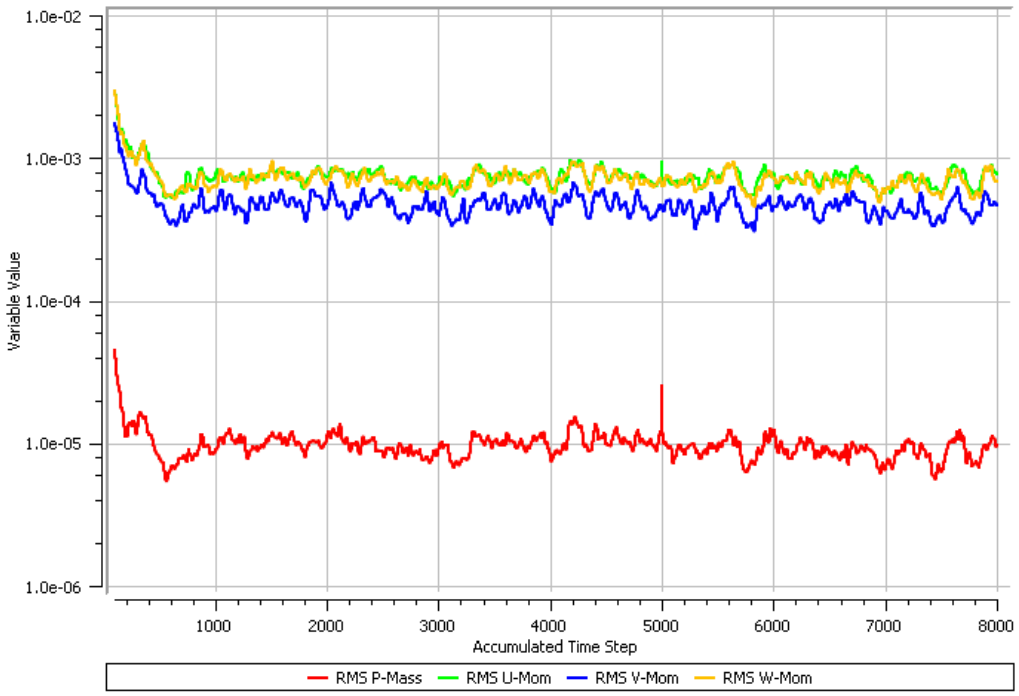

(a) : The mass and momentum simulation residuals.

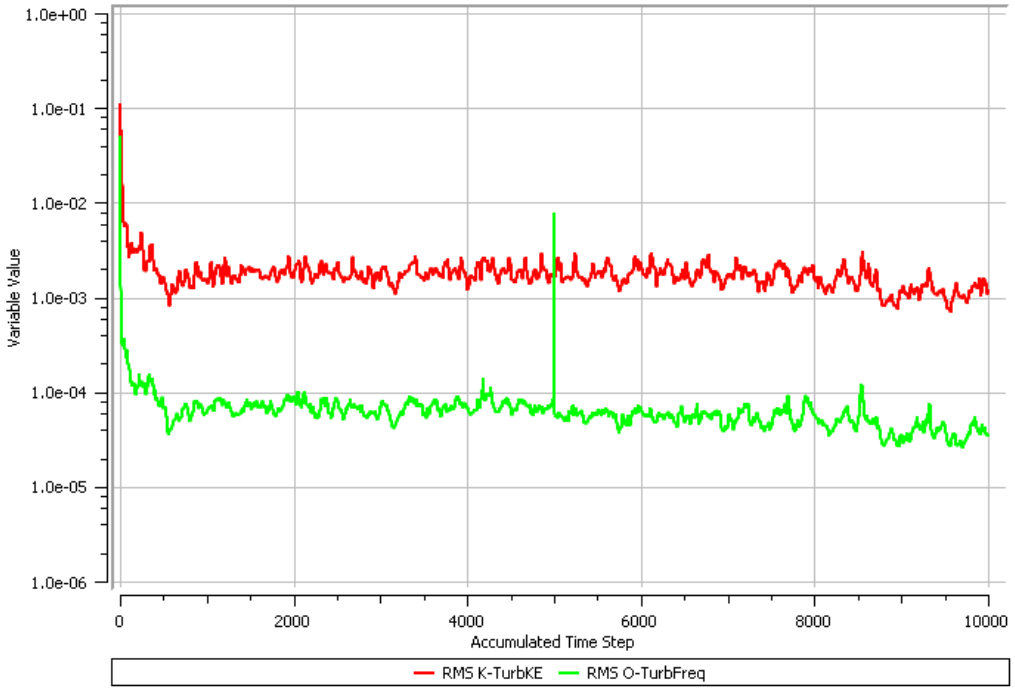

(b) : The turbulence values.

Figure 3.3: CDF simulation residuals outputs for 10 % EG mixture at 55° C.

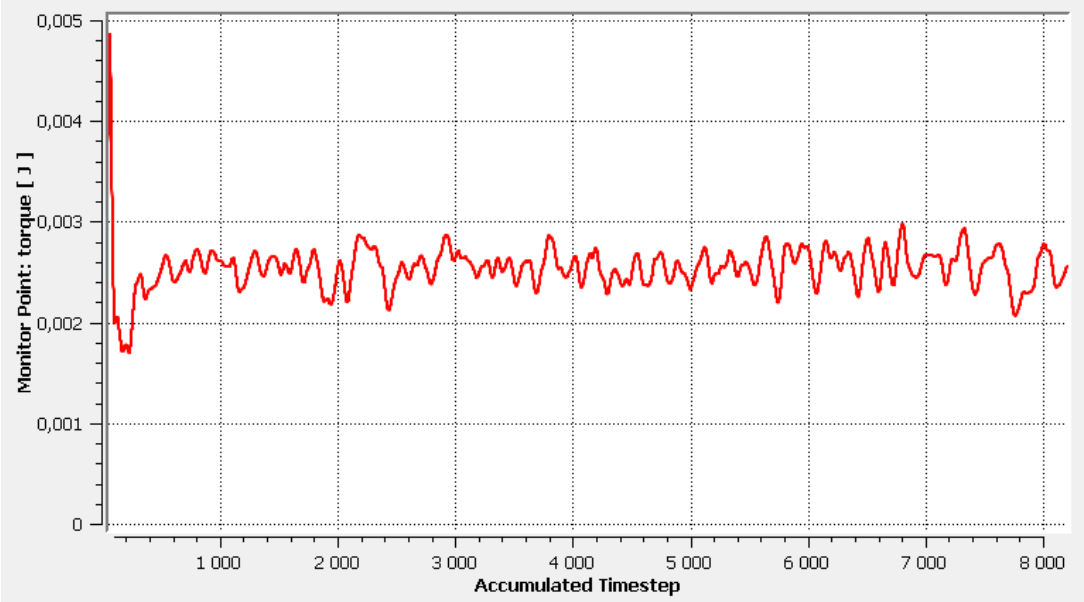

Figure 3.4: The pump impeller output torque for 10 % EG mixture at 55° C.

3.3 Measurement on real hardware

At the beginning of this section, entire hardware setup of the test pump unit is introduced. Subsequently, the process of measured dataset acquisition, validation and evaluation is described. This source of data is used for fluid detection and parameter estimation on experimental pump setup.

3.3.1 Testbench

Since whole experiment takes place in the pump casing itself the test bench is not particularly difficult. It is composed of a centrifugal pump with wet rotor and speed controller, a platinum thermometer and a non-return valve. The circuit is also equipped with a propeller flow indicator. A second pump is used to ensure the circulation of water providing heating or cooling of the mixture in the test circuit. The physical form is presented in Figure 3.5.

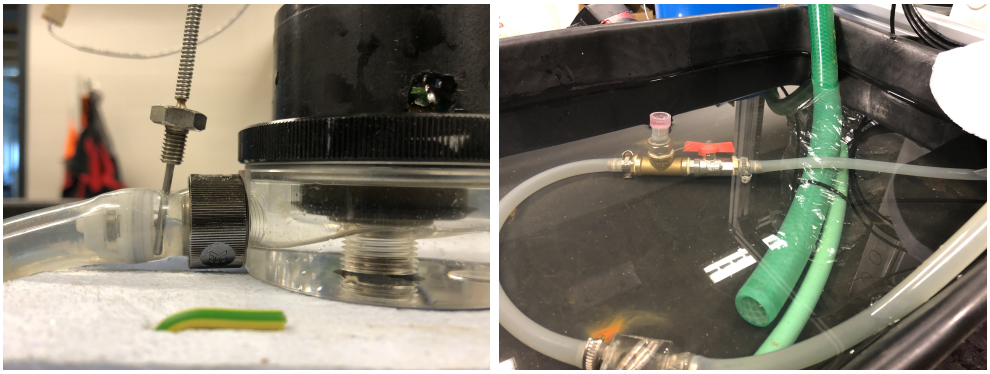

(a) : Centrifugal pump detail. **(b) :** Water tank with test circuit.

Figure 3.5: Physical test-bench.

3.3.2 Power probability distribution

Since the real hardware setup is a stochastic system, the power measurement are impaired noise and has to be represented by some probability distribution. For the distribution analysis, three distinct measurements with constant rotor velocity are made. Firstly, six different water-ethylene glycol mixtures at temperatures 25 °C, 40 °C and 55 °C are measured. Secondly, the pump power at constant water temperature is measured. Lastly, the experiment is reproduced in the same way but with increasing water temperature in the range from 25 °C to 50 °C. The sample of measured dataset, obtained from Simuling model which ensure control of real hardware can bee seen in Figure 3.6. The steps in pump velocity used to mix the liquid in the measuring circuit in order to change the solution temperature.

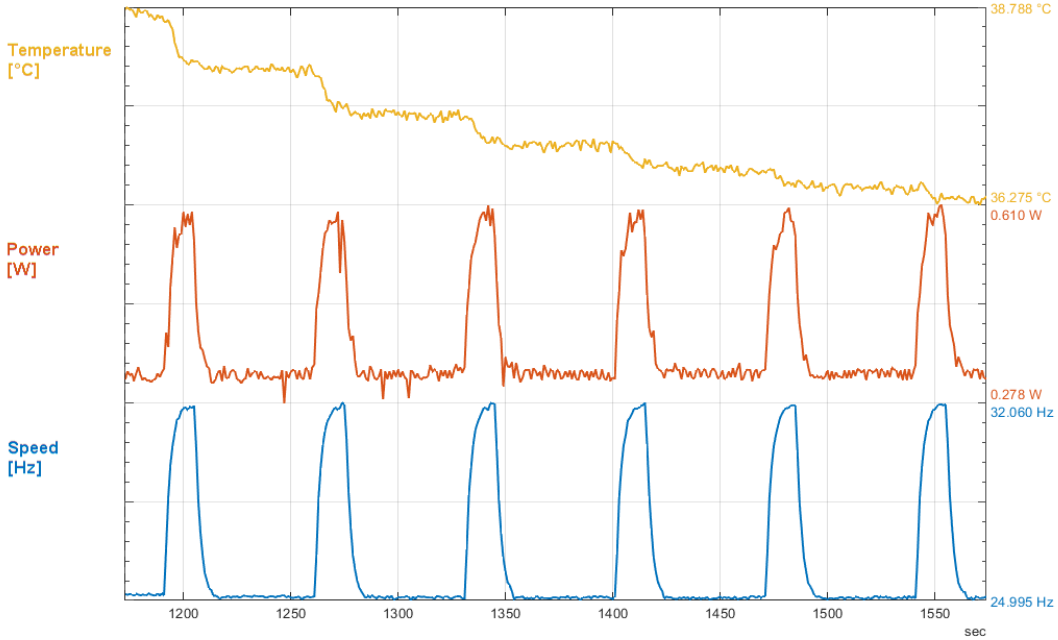

Figure 3.6: Dependency of Ethylene Glycol dynamic viscosity.

Initially, the probability distribution type is determined. The measured power is fitted using the function `histfit`[2] with two probability distributions. These fits can be seen in Figure 3.7. After the fit quality evaluation, an alternative distribution is chosen. Upon analysing the histogram properties of the measured power the t Location-Scale distribution is selected as suitable because a non-negligible weight outside two sigma has been detected.[13]

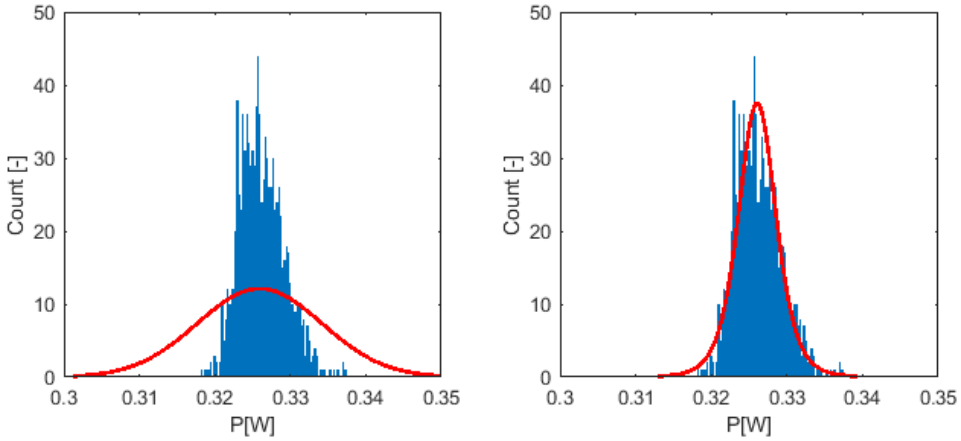

(a) : Fit by normal distribution. **(b) :** Fit by $\mathcal{T}$ distribution.

Figure 3.7: Pump power distribution fit at constant speed and temperature.

The mean of measured data must be subtracted to allow comparison of the distribution properties. Due to this unification the parameters of the $\mathcal{T}$ distribution can be compared across the measurements with different mixture concentration and temperature.

The standardized data are used to fit distributions for all datasets. The distribution parameters obtained by function `fitdist`[3] are compared across the experiments. Resulting parameters differ only in the shape parameter υ. After comparison with validation data, the first measurement is burdened with greater noise because the shape parameter υ is half the size than in case of validation dataset. This is probably caused by the usage of unshielded pump power wires during the first measurement. In order to increase the robustness of fluid detection and estimation algorithms, the lowest shape distribution factor is used. The specific values of distribution parameters used in fluid detection and parameter estimation algorithms are listed in Table 3.3.

Parameter	Values
μ	Power dependent value
σ	0.00472525 [0.00455113, 0.00490602]
υ	2.60471 [2.39199, 2.83634]

Table 3.3: The $\mathcal{T}$ distribution parameters with confidence intervals [13].

[2] `https://www.mathworks.com/help/stats/histfit.html`
[3] `https://www.mathworks.com/help/stats/fitdist.html`

3.4 Model of pump behaviour

This section outlines the procedure of creating a pump behaviour model for detection and estimation purposes. It starts with an introduction of the model operating properties. In the following subsections, all of the necessary obtained model types are presented.

3.4.1 Model properties

The model based on a real power measurement assumes the following behavioural properties. The temperature is deterministic variable without process or measurement noise. Based on subsection 3.3.2, the $\mathcal{T}$ distribution with fixed σ and υ is used for the pump power modelling. Also, the pump operates at constant speed set-point. The pump velocity is burdened only with measurement noise $e \sim \mathcal{N}(0, \sigma)$.

3.4.2 Viscosity model

Based on fluid viscosity influence on pump performance, discussed in section 2.3.2, it is evident that an analytical model formulation of this phenomena is not feasible. For this reason, the fluid viscosity model has been created as linear function of pump power. As expected, this model will work properly only in relatively limited viscosity range. Nevertheless, for the detection and estimation algorithm design, the viscosity range size is not relevant. For the improvement of the estimates quality in a larger range, a better model must be generated. This can be achieved by using superior CFD simulations or a measurement for more various liquid viscosity. The fluid kinematic viscosity for all training mixtures has been generated by CoolProp library. These has been used as independent variables for evaluation of power dependency for CFD as well as real pump measurement. The fluid kinematic viscosity is fitted with polynomial:

$$\nu(P_E) = a_0 + a_1 P_E, \tag{3.2}$$

where P_E is electric power. The resulting fit is depicted in Figure 3.8. The polynomial parameters are listed in Table 3.4.

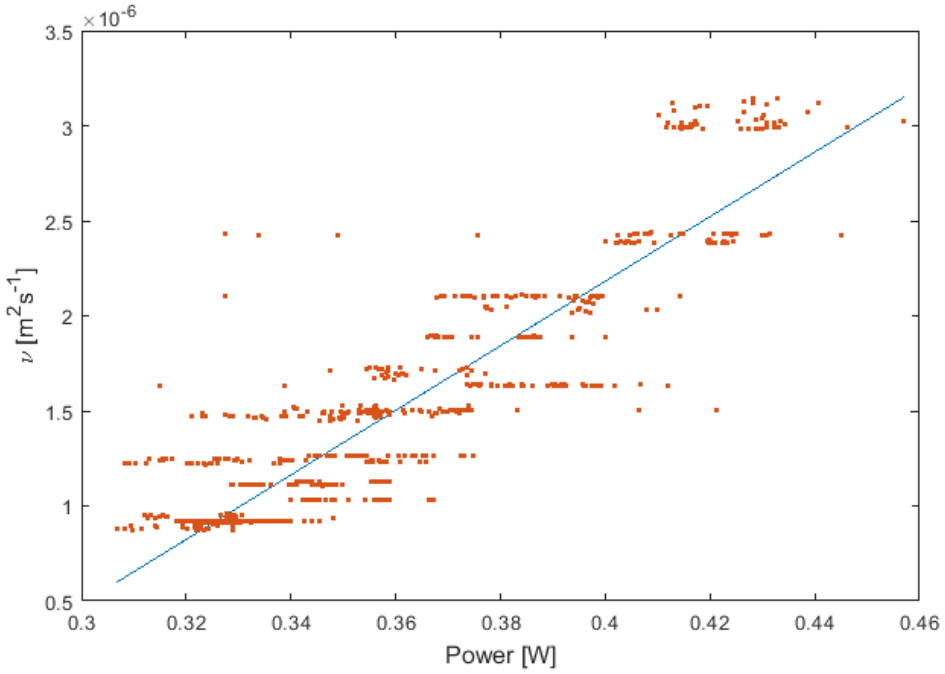

Figure 3.8: The dependency of fluid viscosity on pump power.

Parameter	Values
$\hat{a_0}$	0.000249523 [8.72262e-05, 0.00041182]
$\hat{a_1}$	2.60471 [2.39199, 2.83634]

Table 3.4: The transformed viscosity $\mathcal{T}$ distribution parameters.

Due to uncertainties in polynomial parameters, the estimated viscosity variance must be established. Since it is problematic to determine this dependence analytically, the random sampling method has been used. The power samples are drawn from their $\mathcal{T}$ distribution by transforming the random variable $u \sim \mathcal{U}(0,1)$ by inverse of cumulative distribution function.

Because of possible non-zero polynomial parameters cross-correlation, the covariance matrix is calculated from `polyfit`[4] error structure as follows:

$$\Sigma = \frac{1}{df}(R^{-1} \times R^{-T}) \times norm^2, \tag{3.3}$$

where df represents degrees of freedom, R is triangular factor from a QR decomposition of the Vandermonde matrix of independent variables and $norm$ is the residuals norm. The samples of polynomial parameters are generated from following bivariate standard normal distribution:

$$\begin{pmatrix} a_0 \\ a_1 \end{pmatrix} \sim \mathcal{N}\left(\begin{pmatrix} \hat{a_0} \\ \hat{a_1} \end{pmatrix}, \Sigma\right) \tag{3.4}$$

[4] `https://uk.mathworks.com/help/matlab/ref/polyfit.html`

using multivariate normal random generator `mvnrnd`[5] to avoid adding new prior information.

The random sampling is evaluated on ten equally distributed power locations in range of training dataset. 100 000 power samples have been generated from each location, and they have been randomly transformed by polynomial model with parameters a_0 and a_1. For each power location μ, a histogram of transformed viscosity has been devised. These samples have also been fitted with `fitdist`. In this case, the $\mathcal{T}$ distribution has also been used. The simulated σ and υ parameters can be seen in Figure 3.9.

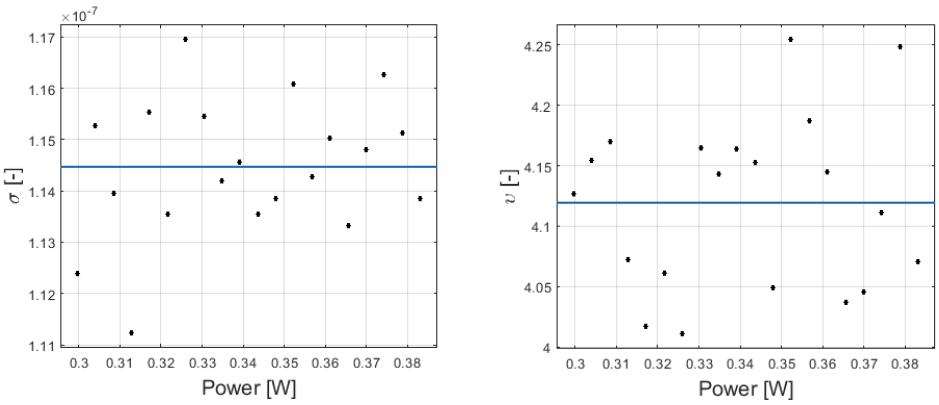

(a) : The scale parameter σ of viscosity distribution.

(b) : The shape parameter ν of viscosity distribution.

Figure 3.9: The estimated parameters of viscosity distribution.

Resulting scale and shape parameters of the viscosity distribution are considered constant and are listed in Table 3.5.

Parameter	Values
σ	1.144e-07 [1.14e-07, 1.147e-07]
υ	4.052 [4.027, 4.078]

Table 3.5: The viscosity t Location-Scale distribution parameters.

3.4.3 Viscosity model for EG solution

The second model has been applied for evaluating kinematic viscosity of water-EG binary solution. It has been used for fast evaluation of the fluid viscosity. The CoolProp library has been employed as a data source for polynomial fitting by the following model:

$$\nu(T, C) = a_0 + a_1 T + a_2 c + a_3 \frac{C^2}{T} + a_4 T^2 C^2 + a_5 T^2 + a_6 C^2 + a_7 T^3 \tag{3.5}$$

where T is mixture temperature and C is volume concentration. The quality of fit is exceptionally high, with values $R^2 = 0.9987$ and $RMSE = 3.7584\text{e}{-8}$. For this

[5] `https://www.mathworks.com/help/stats/mvnrnd.html`

reason, this model has been used as source of fluid true viscosity for detection and estimation. The performance of fluid viscosity has been evaluated by `runperf`[6]. In case of evaluation over 1000 viscosity samples, the polynomial model (0.20668 s) is four time faster than evaluation based on direct access to CoolProp (0.87063 s).

[6] `https://www.mathworks.com/help/matlab/ref/runperf.html`

Chapter 4

Heat transfer media detection

In this chapter, the development and validation of methods used for heat transfer media detection or fluid properties estimation is outlined. The methods and their validation are listed in the following sections.

4.1 Fluid detection

This section presents the developed algorithm for fluid model detection based on training datasets. Fluids models are represented as probability distribution functions that are used in likelihood ratio test. Secondly, the test quality is determined. And lastly, the validation results are discussed.

4.1.1 Water detection

The detection of water presence as a heat transfer medium has been carried out by implementing log likelihood ratio test. For N independent samples the test is defined follows:

$$S = \sum_{k=1}^{N} ln \frac{p_0^k(y(k))}{p_1^k(y(k))}, \tag{4.1}$$

where hypotheses H_0 and H_1 correspond to populations with probability distributions p_0 and p_1. In the case of fluid detection, the t Location-Scale distribution has been used since it is useful for modelling distributions with heavier tails than the normal distribution.[13]

Based on observations of power and viscosity properties in section 3.4.2, distributions with fixed scale σ and shape υ parameters have been utilized. This test has been used to detect the change of location parameter μ, which depends on fluid viscosity. The non-linear map of actual water viscosity is obtained by setting concentration C to zero in the EG viscosity model presented in section 3.4.3.

Due to viscosity temperature dependency, the p_0 and p_1 have been determined independently for each test sample. As a result, it is possible to run this detection algorithm at various fluid temperatures. The distribution p_0 is created as probability distribution object[1] with μ corresponding to pure water viscosity at actual temperature. Further, alternative hypothesis H_1 has been formulated in the same manner with

[1] `https://www.mathworks.com/help/stats/makedist.html`

the difference, that the location of distribution has been calculated as $\Delta\mu = \bar{d} \cdot \mu_W$, where $\bar{d} \in \{0.1, 0.05, 0.01\}$ is viscosity deviation factor and μ_W is appropriate water viscosity.

To allow the detection of less or high viscous fluids, two alternative hypotheses, with locations μ placed in axial symmetry around the null hypothesis, have been used. The principle is depicted in Figure 4.1.

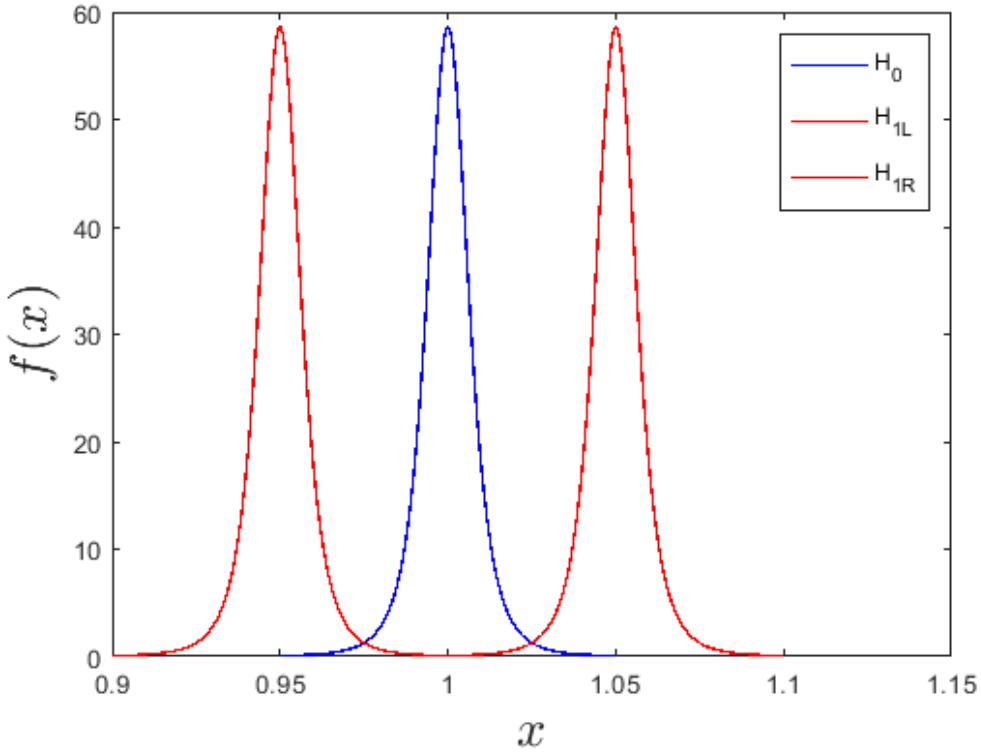

Figure 4.1: The probability density functions of detection hypotheses.

So two likelihood ratios are used. The parameters α and β described in section 2.4.3 are set to equal. As a result, the sing change detection of two sums of likelihood ratios is performed.

$$S_L(N) = \sum_{k=1}^{N} ln \frac{p_0^k(y(k))}{p_{1L}^k(y(k))} \tag{4.2}$$

$$S_R(N) = \sum_{k=1}^{N} ln \frac{p_0^k(y(k))}{p_{1R}^k(y(k))} \tag{4.3}$$

The water hypothesis H_0 is accepted when $S_L > 0$ & $S_R > 0$. Otherwise, the null hypothesis is rejected.

4.1.2 Test quality

The significance level and power of the test is discussed in this section. Randomly generated test data have been used due to the impossibility to measure sufficient amount of validation datasets. The samples generation from pump power distribution is based on usage of inverse CDF obtained from MATLAB probability distribution object. The measured temperature is also created randomly and is obtained as a sum of equidistantly spaced vector in selected temperature range and random values from uniform distribution $\mathcal{U}(-1, 1)$. The procedure form of temperature samples generation has been selected in order to properly simulate temperature caused by spontaneous cooling during real measurement.

The significance and power of test with general $\mathcal{T}$ distribution can be easily analytically calculated for one sample, however, the effect of sample size N, when taken into account, is problematic. The theory of calculation test significance and power for multiple samples described in subsection 2.4.3 can be only used for standard normal distribution. For this reason, the test quality is estimated by numerical simulation over various batch sample sizes and different mean value distances between hypotheses H_0 and H_1.

The sample size is evaluated over sample count determined as 2^k where $k \in \mathbb{Z}$ in range from 0 to 11. The simulated difference of a fluid viscosity is $\Delta\nu = x$ where $x \in \{0.1, 0.05, 0.02, 0.01\}$. The output of numerical solution is the count of both error types over 10 000 iterations. These results are apply to determine three distinct models interpolated with cubic interpolation. Resulting models are used for obtaining the test properties.

For example, parameter α in case of known viscosity deviation $\bar{d}$ and sample size n is returned. Such model can be seen in Figure 4.2.

4.1.3 Validation results

Finally, the last part of fluid detection is the algorithm evaluation on validation datasets. The sample size of validation batch has been determined by model mentioned in subsection 4.1.2. All results of datasets hypothesis testing are listed in Table 4.1. The properties of petrol cleaner that has been used for detection, are found in technical list[2]. As can be seen in Table 4.1, the water hypothesis with a viscosity difference

Fluid	$\bar{d}$	$\alpha\|\beta$	N	**Decision**
Water	0.1	0.05	140	H_0 Accepted
Water	0.05	0.05	140	H_0 Rejected
Petrol cleaner	0.05	0.05	140	H_0 Rejected
EG mixture (C = 0.032)	0.05	0.05	140	H_0 Rejected
EG mixture (C = 0.08)	0.05	0.05	140	H_0 Rejected

Table 4.1: The results of fluid detection validation.

of 5 % has been incorrectly rejected. The incorrect decision is caused by viscosity mean shift close to one of H_1 hypotheses. For this reason, the estimated test power,

[2] `http://www.severochema.cz/files/bezpecnostni-listy/Benzinovy_cistic_technicky.pdf`

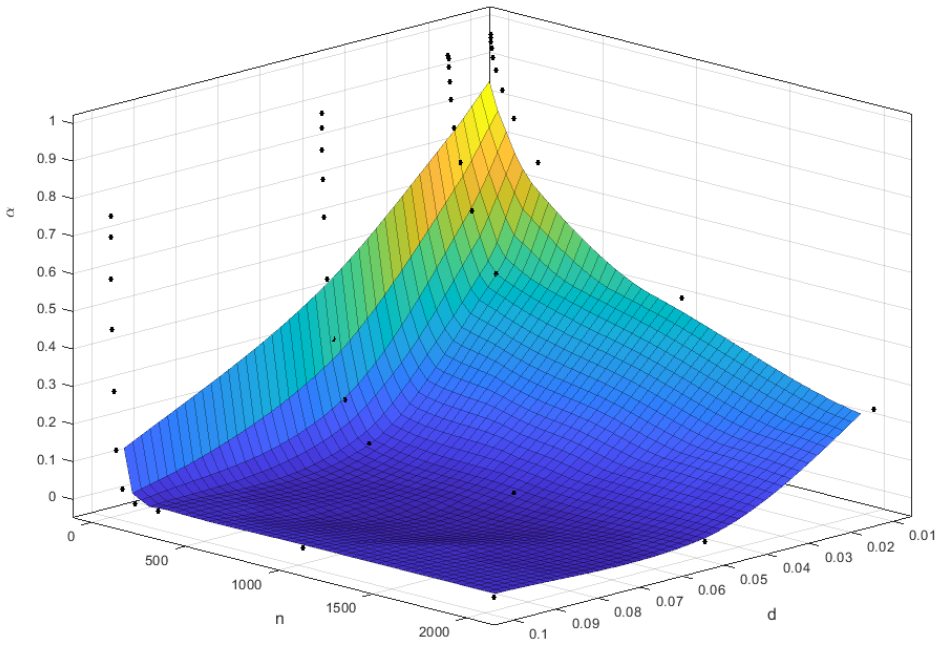

Figure 4.2: The interpolated model of test significance α with ($\alpha = \beta$), dependency on viscosity deviation factor $\bar{d}$ and sample size N.

sample size and significance level do not precisely correspond. This could be caused by a change in the measured power mean during validation or due to model inaccuracies.

This problem can be solved by using a larger sample size. Firstly, the change of detected mean of fluid viscosity can be caused by the motor winding heating whose compensation is not yet included in the control. Secondly, the viscosity drift could also be generated by penetration of air bubbles into the pump wet rotor.

4.2 Mixture concentration estimation

Firstly, the process of estimation the water-ethylene glycol mixture concentration is described. Secondly, the validation of estimated concentration has been carried out. Lastly, the validation results have been discussed.

4.2.1 Concentration estimate

The stochastic model of fluid viscosity can be described by following equation:

$$\boldsymbol{\nu} = f(\boldsymbol{T}, C) + \boldsymbol{e}, \tag{4.4}$$

where f is deterministic part of model and e is random variable $e \sim \mathcal{T}(0, \sigma_\nu, \upsilon_\nu)$. The model can be alternatively expressed as $\boldsymbol{\nu} = g(\boldsymbol{e})$. In order to analyse a probability

p_ν, the univariate transformation is expressed as:

$$p_\nu = p_e(g^{-1}(\boldsymbol{\nu})) \left| \frac{\partial}{\partial \boldsymbol{\nu}} g^{-1}(\boldsymbol{\nu}) \right|, \tag{4.5}$$

where function g^{-1} is defined as $\boldsymbol{e} = g^{-1}(\boldsymbol{\nu}) = \boldsymbol{\nu} - f(\boldsymbol{T}, C)$. Thereafter, the conditional probability is in form as follows:

$$p_\nu(\boldsymbol{\nu}|\boldsymbol{T}, C) = p_e(\boldsymbol{\nu} - f(\boldsymbol{T}, C)). \tag{4.6}$$

Since probability distribution is preserved by univariate transformation, the resulting distribution of conditional probability function p_ν is the same as for the random variable e, which can be expressed as:

$$p(\boldsymbol{\nu}|\boldsymbol{T}, C) = \frac{\Gamma\left(\frac{\upsilon+1}{2}\right)}{\sigma\sqrt{\upsilon\pi}\,\Gamma\left(\frac{\upsilon}{2}\right)} \left[\frac{\upsilon + \left(\frac{\boldsymbol{\nu} - f(\boldsymbol{T}, C)}{\sigma}\right)^2}{\upsilon} \right]^{\left(\frac{\upsilon+1}{2}\right)}, \tag{4.7}$$

where ν is viscosity, υ is distribution shape factor, function $f(T, C)$ is a polynomial obtained by evaluating ethylene glycol viscosity model described in subsection 3.4.3 at selected temperature. The polynomial is in form:

$$f(\boldsymbol{T}, C) = a_2(\boldsymbol{T})C^2 + a_1(\boldsymbol{T})C + a_0(\boldsymbol{T}). \tag{4.8}$$

Ultimately, the resulting likelihood function is formulated in accordance with subsection 2.4.5 as:

$$ln\, \ell(C|\boldsymbol{\nu}, \boldsymbol{T}) = \sum_{i=1}^{N} ln\, \ell(C|\nu_i, T_i). \tag{4.9}$$

The estimated concentration value of ethylene glycol solution is determined as:

$$\hat{C}(\boldsymbol{\nu}, \boldsymbol{T}) = arg \max_C \ell(C|\boldsymbol{\nu}, \boldsymbol{T}). \tag{4.10}$$

The variance of concentration estimate can be obtained by solving equation:

$$P_{\hat{x}} = - \left(\frac{\partial^2 ln\, \ell(C|\boldsymbol{\nu}, \boldsymbol{T})}{\partial^2 C} \right)^{-1}, \tag{4.11}$$

at $\hat{C}$. The second derivative can be written in form as follows:

$$\begin{aligned} \frac{\partial^2 ln\, \ell(C|\boldsymbol{\nu}, \boldsymbol{T})}{\partial^2 C} = (\upsilon + 1) \sum_{i=1}^{N} \Bigg[& \frac{[-(2a_{2i}C + a_{1i})^2 + 2a_{2i}(\nu_i - f_i(C))]}{[\upsilon\sigma^2 + (\nu_i - f_i(C))^2]} \\ & \frac{[\upsilon\sigma^2 + (\nu_i - f_i(C))^2]}{[\upsilon\sigma^2 + (\nu_i - f_i(C))^2]} \\ & + \frac{2(2a_{2i}C + a_{1i})^2(\nu_i - f_i(C))^2}{[\upsilon\sigma^2 + (\nu_i - f_i(C))^2]} \Bigg], \end{aligned} \tag{4.12}$$

where $f_i(C)$ is evaluated function $f(\boldsymbol{T}, C)$ at actual temperature sample.

4.2.2 Numerical implementation

The numerical estimation algorithm is developed consistently with subsection 4.2.1. It is implemented by nested function used for evaluating likelihood for entered volume concentration. The sum of probability density of each independently transformed power sample is calculated. The conditional t Location-Scale distribution is created consistently to subsection 3.4.2 with fix scale and shape parameters. The location parameter is determined from the ethylene glycol viscosity model which can be found in subsection 3.4.3. The estimator working principle is shown in Figure 4.3.

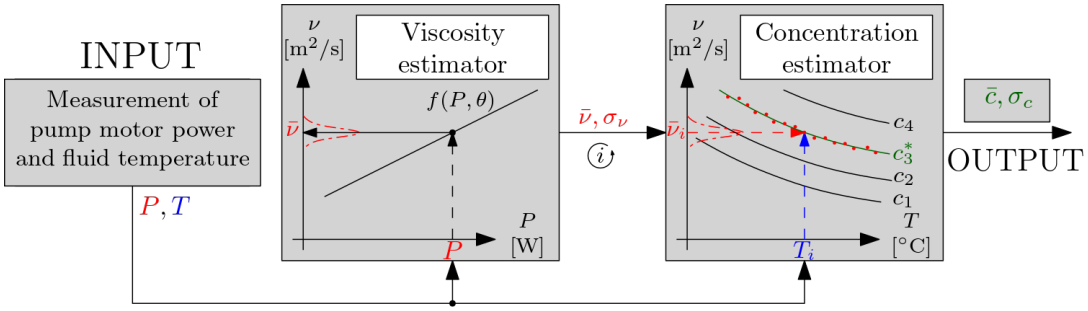

Figure 4.3: The operating principle of fluid solution concentration estimation.

The nested function is then used by `MultiStart`[3] object. Despite the fact, that the likelihood function should be monotony, the parallel multi-start approach is used.

4.2.3 Estimation variance

The variance of concentration estimate is obtained as numerical differentiation of nested function by using `hessian`[4] which is a part of Adaptive Robust Numerical Differentiation toolbox[22].

The estimate variance should be verified because of possible errors caused by using numerical differentiation. This is done by comparing the concentration variance over other two distinct methods.

The first method is based on analytically calculated hessian of likelihood function introduced by equation (4.12). The variance of concentration estimate has been obtained by solving the equation (4.11) at estimated value $\hat{C}$. The value of calculated variance is 2.032e−5.

Secondly, the Monte Carlo random sampling method has been implemented. The 150 samples of pump power operating dataset with specific mixture concentration have been generated. These randomly generated samples have been transformed by the viscosity model and evaluated by the concentration estimator. Thereafter, the histogram of 5000 evaluated estimates can be seen in Figure 4.4. It has been fitted with standard normal probability distribution with $\mu = 2.192\text{e}{-1}$, $\sigma = 6.011\text{e}{-3}$ and variance 3.613e−5. The mean of variance vector based on numerical hessian evaluated in each iteration is 1.457e−5.

[3] `https://www.mathworks.com/help/gads/multistart.html`
[4] `https://www.mathworks.com/matlabcentral/fileexchange/13490-adaptive-robust-numerical-differentiation`

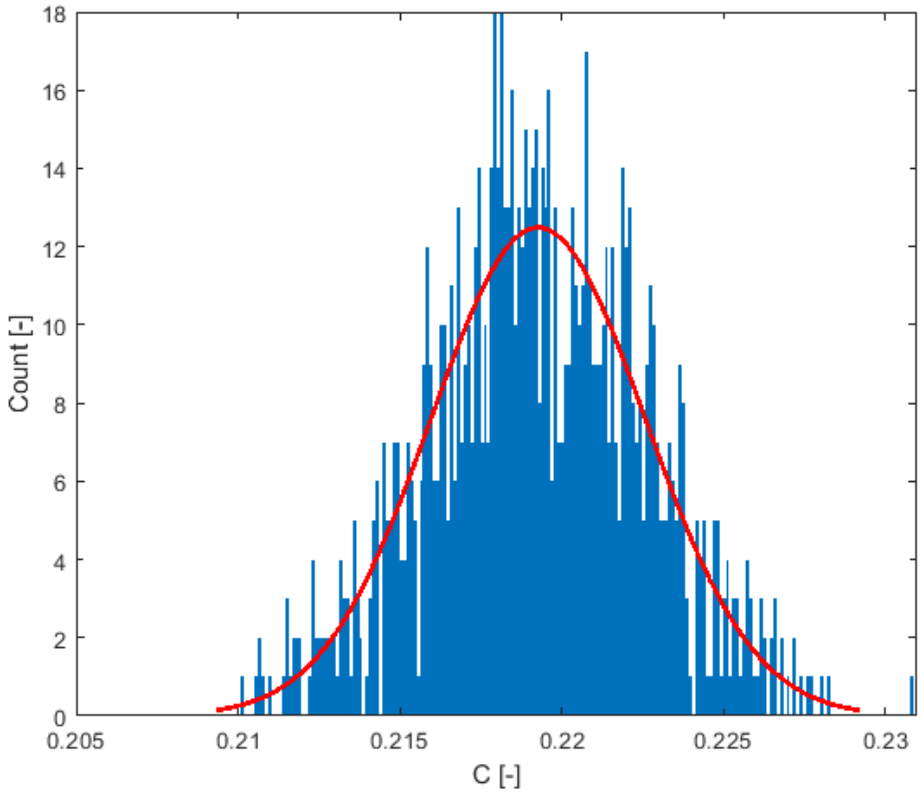

Figure 4.4: The histogram of concentration estimates for 0.2 volume EG concentration.

As can be seen from calculated variances of estimates, values across all above-mentioned methods have same order only with the difference in resulting variances. The dissimilarity is most likely caused by insufficient sample count in case of random sampling and numerical errors during computations.

4.2.4 Validation results

For validation, ethylene glycol mixtures with various volume concentrations have been used. The complete results are listed in Table 4.2. The illustration of resulting function can be seen in Figure 4.5.

Volume concentration	$\hat{C}$	$var(C)$
0 %	3.01 %	4.566e−6
20 %	15.35 %	1.368e−5
8 %	28.96 %	1.0563e−5
13 %	37.16 %	4.305e−6

Table 4.2: The results of ethylene glycol concentration estimation.

As can be seen in Table 4.2, the last two estimates differ perceptibly. The difference

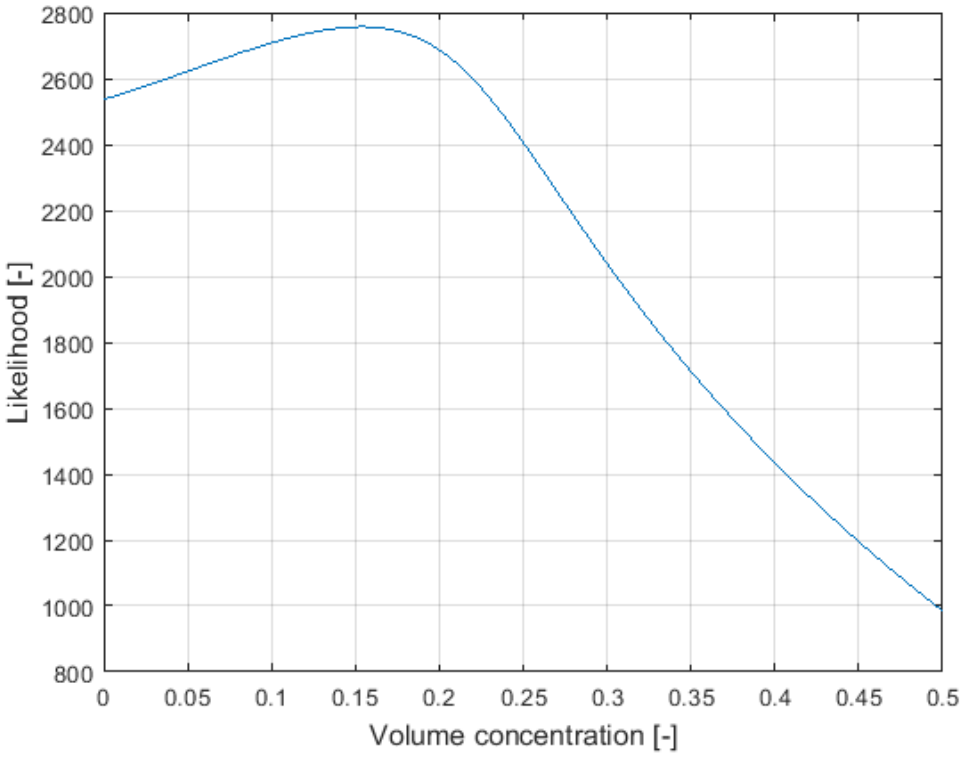

Figure 4.5: The likelihood function evaluated on concentrations $(0, 0.5)$ with step 0.005 %. Validation fluid EG with 0.2 volume concentration. MLE output is $\hat{C} = 15.35$ %, $var(C) = 2.046\text{e}{-5}$.

is caused by an increase in the mean of the pump power for hitherto unknown reasons. Same as in subsection 4.1.3, the heating of the motor winding is probably responsible for the power mean drift. Since these are only assumptions, it would be ideal to incorporate the winding temperature estimation and compensation into the power measurement.

4.3 Fluid viscosity model estimation

The viscosity of pumped fluid used in previous detection and estimation algorithm can also be used separately, without the knowledge of fluid or mixture properties. Based on observation in subsection 3.4.3, the `polyfitn` function has been applied. The fitted model of kinematic viscosity over dataset has been represented as polynomial in form as follows:

$$\nu(T) = a_0 + a_1 T + a_2 T^2 + a_3 T^3. \tag{4.13}$$

Since the laboratory is not equipped with any rheometer, the resulting model of viscosity cannot be validated for various fluid types. Obviously, it is possible to obtain different types of fluid with known properties from CoolProp. However, these measurements are not optimal for proper validation of viscosity estimation.

Chapter 5

Conclusion

Nowadays with increasing costs of energy, the control of buildings' heating or cooling should be done effectively. An innovative approach using active one-pipe architecture brings the possibility of optimizing the costs of the building's heating or cooling. The efficient control is conditioned by accurate knowledge of heat flow. An affordable approach implies using the flow estimation without the application of flow meters. The current heat flow estimate algorithm described in the patent [3] could be further improved by the knowledge of specific heat capacity of the transported fluid and thus the thesis focuses on estimating the fluid properties.

Firstly, in this thesis, the theoretical analysis of fluids and their effects on centrifugal pumps have been discussed. Since the analysed system consists of deterministic and stochastic part, statistical approach is selected. This approach allows the development of pump model behaviour for distinct fluid viscosities. Subsequently, the power-viscosity model is used for detection and estimation algorithms.

The developed virtual sensor of fluid viscosity is firstly used for detecting the water presence as a pumped media. The likelihood ratio test has been selected because of its properties suitable for this task. The resulting fluid detection validated on real measurements is correct in the majority of cases. The second application of the developed virtual sensor is solution concentration estimation. The volume concentration estimates are validated only on EG solution due to its availability and implementation in CoolProp library.

The fluid model based on different solution can be used without any modifications in the detection and estimation algorithms. For this reason, validation of distinct fluid concentration estimation is effortless. The detected viscosity can be also used separately without prior knowledge of fluid properties.

Thanks to the successful concept validation on a micro centrifugal pump, assumption based on theoretical knowledge promotes the idea, that identically detectable phenomena will occur in case of larger centrifugal pumps. Therefore, the deployment in wider application field, where centrifugal pumps are commonly used, could be possible. In industrial systems with requirements for larger flow, non-return spring valve could be restrictive. On the other hand, when the flow is measured by flow meter, the viscosity estimation might be possible even in case of non-zero flow. This modification could allow fully continual viscosity estimation.

Bibliography

[1] O. Zlevor and J. Dostál, "Demand-oriented hydronic heating system and the active one-pipe system design tool," *E3S Web of Conferences*, vol. 111, p. 01091, 01 2019.

[2] J. Dostál and T. Bäumelt, "Model predictive control for buildings with active one-pipe hydronic heating," *E3S Web of Conferences*, vol. 111, p. 04050, 01 2019.

[3] T. Bäumelt, J. Dostál, J. Hauser, J. Kubeš, J. Valtr, and O. Zlevor, "Equipment for heat exchanger power control in a single-pipe heating network," Patent 308 007.

[4] G. B. J. Scott D. Miles, Gill B. Beamson, "Methods and systems for determining a viscosity of a fluid," Patent US7 578 782B2.

[5] W. C. Lloyd C. HubbardEarl, "Flow measurement system," Patent US4 781 525A.

[6] S. B. Alabi, Ph.D. dissertation, 2010. [Online]. Available: https://ir.canterbury.ac.nz/bitstream/handle/10092/5481/thesis_fulltextpdf.pdf?sequence=1

[7] D. S. Viswanath, T. K. Ghosh, D. H. L. Prasad, N. V. Dutt, and K. Y. R. (auth.), *Viscosity of Liquids: Theory, Estimation, Experiment, and Data*, 1st ed. Springer Netherlands, 2007.

[8] G. J. F., *Centrifugal pumps*. Springer, 2010.

[9] D. Papantonis, *Centrifugal pumps*. InTech, 2012.

[10] Khalafallah and Galal, "Disk friction loss in centrifugal and mixed flow pumps," 12 2001, pp. 1–7.

[11] R. Torabi and S. A. Nourbakhsh, "The effect of viscosity on performance of a low specific speed centrifugal pump," *Hindawi Publishing Corporation*, pp. 1–10, Jun. 2016.

[12] K. Siegrist, "Location-scale families," [Online; accessed 10-March-2020]. [Online]. Available: http://www.randomservices.org/random/special/LocationScale.html

[13] MathWorks, "t Location-Scale Distribution," https://www.mathworks.com/help/stats/t-location-scale-distribution.html, 2020, [Online; accessed 10-March-2020].

[14] R. S. Witte and J. S. Witte, *Statistics*. Wiley, 2017.

[15] S. L., "Power and Sample Size Determination," http://sphweb.bumc.bu.edu/otlt/MPH-Modules/BS/BS704_Power/BS704_Power_print.html, [Online; accessed 14-March-2020].

[16] J. A. Rice, *Mathematical statistics and data analysis*. Thomson Brooks/Cole, 2007.

[17] V. Havlena and J. Štěcha, *Moderní teorie řízení*. Vydavatelství ČVUT.

[18] B. I. H., J. Wronski, S. Quoilin, and V. Lemort, "Pure and pseudo-pure fluid thermophysical property evaluation and the open-source thermophysical property library coolprop," *Industrial & Engineering Chemistry Research*, vol. 53, no. 6, pp. 2498–2508, 2014. [Online]. Available: http://pubs.acs.org/doi/abs/10.1021/ie4033999

[19] E. W. Lemmon, I. Bell, M. L. Huber, and M. O. McLinden, "NIST Standard Reference Database 23: Reference Fluid Thermodynamic and Transport Properties-REFPROP, Version 10.0, National Institute of Standards and Technology," 2018. [Online]. Available: https://www.nist.gov/srd/refprop

[20] Wikipedia, "Ethylene glycol — Wikipedia, the free encyclopedia," http://en.wikipedia.org/w/index.php?title=Ethylene%20glycol&oldid=951647244, 2020, [Online; accessed 10-April-2020].

[21] Ansys, "Ansys CFX," https://www.ansys.com/products/fluids/ansys-cfx, 2020, [Online; accessed 15-February-2020].

[22] J. R. D'Errico, "Adaptive Robust Numerical Differentiation," https://www.mathworks.com/matlabcentral/fileexchange/13490-adaptive-robust-numerical-differentiation, 2020, [Online; accessed 30-April-2020].

Appendix A

Contents of the enclosed CD

The electronic version of the diploma thesis is present on the enclosed CD.